The evolutionary state of stars in the NGC 1333S star formation region

Colin Aspin
Gemini Observatory, 670 N. A'ohoku Place, Hilo, HI 96720
caa@gemini.edu

ABSTRACT

We present 2μm near-IR spectroscopic observations of a sample of 33 objects in the NGC 1333S active star forming cluster centred on the pre-main sequence star SSV 13. We have previously studied this region photometrically in the optical and near-IR and, with the addition of these near-IR spectra, we further probe the pre-main sequence cluster membership and evolutionary state. From the atomic and molecular absorption features observed together with the earlier photometry, we derive spectral types, effective temperatures, masses and ages of the stars and conclude that almost all (90%) the stars observed in this sample are pre-main sequence objects. This result significantly refines the evolutionary information obtained from photometric evidence alone. Comparison with theoretical evolutionary tracks and isochrones suggests that our survey has sampled sources with masses in the range 0.2–2M$_\odot$/ and stellar ages between 7×10^4 and 1×10^8 years with a preponderance of sources around 3×10^6 years. This implies the presence of low- to intermediate mass T Tauri stars of evolutionary designation Class I to Class III. We conclude that star formation seems to have occurred in likely several bursts rather than occurring coevally. Star formation in such a region as NGC 1333S is likely significantly affected by the large number of active molecular outflows in the region which could provide a mechanism for cloud turbulence and the onset of subsequent star formation.

Subject headings: stars: formation – circumstellar matter – ISM: individual NGC 1333 – stars: pre-main sequence – dust, extinction – infrared: stars – spectroscopy

1. Introduction

If we are to better understand the processes by which star formation is initiated and stars form and evolve, it is necessary to observationally characterize the size, composition and age of pre-main sequence (PMS) stellar populations for individual star formation regions (SFRs) in many different star formation environments. Numerous observational results of such studies have been published. Many surveys have concentrated on the global statistical properties of the regions (see for example the pioneering near-IR surveys by Lada et al. 1991a and Lada et al. 1991b of M17 and L1630, respectively) due to the large number of sources detected, while others have attempted to investigate the characteristics of individual members of less populous region (for example the Serpens survey by Eiroa & Casali 1992).

We have previously presented results on a near-IR (NIR) survey of the region NGC 1333S (cf. Aspin, Sandell & Russell [ASR] 1994, henceforth Paper I, and Aspin & Sandell 1997 henceforth Paper II). Highly active intermediate- to low-mass star formation is occurring in NGC 1333Swhich consists of a region some $10'\times10'$ in extent, located in the L1450 dark cloud complex of Perseus OB2 (Sargent 1979) and centred on the well known, young, PMS object SSV 13[1]. We adopt a distance to NGC 1333S of 318pc based on the *Hipparcos* parallactic measurements of the Perseus

[1] We adopt the SSV designation for this source following the Herbig & Jones (1983).

OB2 association (de Zeeuw 1999). NGC 1333S and its companion region NGC 1333N (located $\sim 10'$ north-east of NGC 1333S) have been the subject of numerous observational campaigns spanning over 20 years, specifically, in the optical/NIR (cf. Strom, Vrba & Strom 1976; Strom et al. 1986; Ladd et al. 1993, 1994; Paper I; Lada, Alves & Lada [LAL96] 1996; Paper II), in the mid/far-IR (FIR; Harvey et al. 1984; Jennings et al. 1987) and in the mm/sub-mm (Bachiller & Cernicharo 1986; Liseau, Sandell & Knee 1988; Warin et al. 1996; Sandell & Knee 2000). Both regions have been shown to contain a significant population of young, PMS objects with ages ranging from $\sim 10^4$ years (Saraceno et al. 1996) to a 1–2$\times 10^6$ years (LAL96) i.e. objects ranging in evolution from extremely young, highly embedded and active accretion/outflow (Class 0/I) sources (e.g. IRAS2 – Sandell et al. 1994, Ward-Thompson et al. 1996; IRAS4 – Sandell et al. 1991, Blake et al. 1995; both sources, Langer, Castets & Lefloch 1996) to ones close to emerging, or recently emerged, from their natal dust/gas cocoons (Class II) and soon to begin main sequence (MS) life (e.g. Lk Hα 271, 352, 355 – Herbig 1974 , SS107 – Strom, Strom & Stocke 1983).

Our work in NGC 1333S have been aimed at i) improving the discrimination between embedded PMS stars and reddened background sources (i.e. stars behind the associated and often dense molecular cloud), and ii) defining in more detail the characteristics of the individual young stars. Since PMS stars both consume (via accretion) and shed (via outflow) their circumstellar obscuring envelopes/disks, their spectral energy distributions (SEDs) evolve (see for example the SEDs of Taurus sources in Kenyon, Calvet & Hartmann 1993), their NIR 'thermal' excess emission (which often easily distinguishes them from reddened background stars) declines and their optical-NIR or NIR colours will become more typical of reddened background sources. Hence, the older a PMS star becomes, the less simple it is to distinguish it from reddened background objects.

Our original NIR JHK survey of NGC 1333S (Paper I) detected 134 sources at K to a 5σ limiting magnitude of 16.2. From NIR J-H vs. H-K (JHK) colour-colour (c-c) diagrams with the additional of optical imaging photometry (R,I) and knowledge of some sources from previous work, we concluded that 55 sources (or 41%) of the stars detected at K were likely PMS objects. These clearly formed a PMS cluster around a location close to SSV 13. The K band sources were individually designated (e.g. ASR 1 is SSV 13) to allow them to be identified for subsequent observations. LAL96 also studied NGC 1333S in the NIR (JHK) as part of a larger scale survey (including NGC 1333N). They detected 275 sources in their 432 square arcminutes survey field (over 4$\times$ larger than the field surveyed in Paper I) and performed a statistical analysis of the PMS population. From the analysis of the dereddened K luminosity function of the PMS stars, LAL96 concluded that the evolutionary state of star formation in NGC 1333 as a whole was more similar to that found in the Trapezium cluster in Orion rather than in the other major SFR in Perseus, IC 348.

Following our work in Paper I, we extended the wavelength range of our survey of NGC 1333S to 3μm attempting to better assess the PMS population by the addition of L band photometry to the earlier JHK data (see Paper II). The L band photometry from NIR array images served to prove the difficulty in obtaining thermal NIR photometry of a complete population of PMS stars. This is mainly due of the high thermal background (telescope+sky) present resulting in a 5σ stellar detection limit in our survey of 12.2. In L we detected only 45% of the sources detected at K, however, these data demonstrated that our original conclusions from Paper I were correct and that the membership of the PMS population found from the JHK photometry was reasonably accurate. The L band data also allowed us to clarified the nature of some sources with previous inconclusive classifications.

An additional approach recently employed to study young stellar clusters has been to observe individual stars spectroscopically. Since many are embedded in the parent molecular cloud and/or their natal stellar envelopes, observations in the NIR are most rewarding. Examples of such studies are Casali & Matthews (1992) who studied CO overtone absorption in 10 low-luminosity young stellar objects (YSOs) in Ophiuchus, Greene & Meyer (1995, henceforth GM95) who presented results on 34 YSOs also in the ρ Ophiuchus dark cloud, Greene & Lada (1996), who presented observations of over 100 sources in Ophiuchus, Taurus and several other nearby SFRs, Luhman et al. (1998) who studied the membership of the IC348 cluster, and Wilking, Greene & Meyer (1999, henceforth WGM99) who studied brown-dwarf candidates in the central high A_V region of ρ Oph. An additional noteworthy treatment of NIR spectroscopy of YSOs is to be found in Meyer (1996).

A spectroscopic approach to the study of PMS populations is clearly important and proven successful in determining the evolutionary information of sources in molecular cloud. We therefore present below a study of the 2μm NIR spectroscopic characteristics of 33 sources in the NGC 1333S region which compliments and extends the original JHKL photometry analysis.

2. Observations and Data Reduction

The NIR spectroscopy presented below was acquired using the Cooled Grating Spectrometer, CGS4 (Mountain, et al. 1990), on the United Kingdom InfraRed Telescope, UKIRT, on Mauna Kea, Hawaii during three nights UT Nov 23 1993, and Dec 27 and 28, 1993. All nights were clear and photometrically stable with 'seeing' of $\sim$0.8–1". CGS4 utilizes a 256$\times$256 Santa Barbara Research Center (SBRC) InSb array and was configured for intermediate-resolution spectroscopy resulting in an R$\sim$1000 at 2.2μm using a 1.2"$\times$90" slit. The spectral range covered by the observations was 2.05 to 2.45μm and the total on-source integration time was 10–30 minutes depending on source brightness. All spectra were sky-subtracted after preliminary processing (bias subtraction, flat-fielding) using blank sky observations taken interspersed between multiple target observations. Sky observations were acquired by sliding the star along the long-slit and hence, object observations were obtained at both spatial positions. Any remaining residual sky emission structure was removed by interpolation perpendicular to the spectral dispersion direction. Data reduction was achieved using the U.K. Starlink FIGARO software package. Target spectra (two per dataset, one positive, one negative due to the subtraction) were optimally extracted (using PROFILE and OPTEXTRACT) from the spectroscopic images and each ratioed by similarly extracted spectra of standard stars acquired close in time and at an equivalent airmass (within 0.1 airmass). This effectively corrected for telluric absorption effects. The standard star spectra were first themselves ratioed by a black-body function of the appropriate effective temperature (using IRFLUX) so that the resultant ratioed target spectrum preserved the target spectral energy distribution. In many cases, two different standard stars were observed per target each being ratioed into the same spectrum to check for difference in the resultant target spectra. No statistically significant differences were detected. All standard stars were of spectral type A or late-F to minimize the number of spectral features present (cf. the spectral classification standard star spectra of Kleinmann & Hall 1986, henceforth KH86). The 2.166μm Brγ absorption line present in the these spectra was removed via linear interpolation prior to their use. Spectra were acquired with an over-sampling of 3$\times$ over 2 pixels to give Nyquist sampled spectra and to complete occasional gaps in the caused by the removal of some bad pixels. The over-sampling was achieved by linear translation of the detector. This can result in a 'ripple' effect in the final source spectrum, due to variations in atmospheric transparency during the acquisition of the six over-sampled observations per set, which manifests as a slight periodic change in signal level throughout the spectrum. When present, the ripple was effectively removed using the FIGARO routine IRFLAT. The spectrometer slit was oriented north-south for all spectra acquired. Wavelength calibration was achieved by observations of an Argon arc. Flux calibration was determined with respect to the standard star spectra and should be considered accurate to $\pm$20%. A more comprehensive discussion of the spectroscopic reduction techniques employed for CGS4 data can be found in Puxley, Beard & Ramsey (1992).

2.1. Target Sample

The 2μm spectra of the 33 sources observed in NGC 1333S are shown in Figs. 1 and 2. Details of these sources e.g. previous identifications, apparent K magnitudes (m_K), classifications from Paper I etc, can be found in Table 1. The individual Figure plots each show spectra of five sources having been normalized to unit intensity at 2.25μm. The sources range in brightness from $7.7 > m_K > 13.5$ and a histogram of their brightness distribution is shown in Fig. 3. The average source brightness in this survey is m_K ∼10–11. Comparison of Fig. 3 with Fig.17 in Paper I shows that we have sampled the brighter end of the m_K luminosity function for the region and have observed 25% of the sources detected. Our K-band luminosity function from Paper I is estimated to be complete to m_K ∼16. Since all spectra are flux calibrated with respect to the standards observed, Table 2 gives the fluxes at the wavelength extremes of the spectral plots and at 2.25μm.

In Paper I, we attempted to determine whether the NIR colours (J-H, H-K) of the sources found were consistent with being reddened (by the molecular cloud) background stars. The classification assigned to the sources observed is indicated by CwR (Consistent with Reddening) in Table 1). Of the 33 sources, 17 were designated CwR=Y while an additional 7 sources were located either close-above (C_A) or close-below (C_B) the reddening lines in the JHK c-c diagram in Paper I. Also given in Table 1 are the derived visual extinction, A_V, for those sources with CwR=Y or designated C_A, C_B together with the implied spectral types, both values from dereddening NIR photometry onto the ZAMS (both from Paper I). The range of A_V values covered by our current sample is $0<A_V<32$ with an arithmetic mean of $\overline{A_V}=7$. This is consistent with the mean from the complete sample of sources found in NGC 1333S in Paper I and in LAL96. The evolutionary classification of the sources from Paper I are also shown in Table 1. Here, a 'Y' indicates that the source was considered a member of the PMS population of stars in the NGC 1333S SFR in Paper I. The number of stars given this designation total 21 and include 10 stars with a CwR=Y designation. These objects are identified as PMS sources from other sources, specifically, those with an overly large distance modulus (from dereddening them onto the ZAMS to obtain a spectral classification), those with an overly small distance modulus (with respect to [wrt] the distance of NGC 1333S i.e. <7.7)[2] and a derived A_V >5, those with associated Hα emission, and those with anomalous optical–NIR colours from an R-I vs. J-K (RIJK) c-c diagram.

[2]In Paper I we assumed a distance to NGC 1333S of 350pc. This was revised to 220pc in Paper II. Here we use the more accurate distance of 318pc from *Hipparcos*.

3. Results

3.1. Spectral features

3.1.1. Atomic and molecular features

The spectra shown in Figs. 1 and 2 show a variety of features representative of either highly reddened (e.g. ASR 106 has a rising red continua) and relatively unreddened (e.g. ASR 56 has a declining blue continuum) sources, sources with either high (e.g. ASR 130 has Brγ absorption) or low (ASR 2 has CO absorption) effective temperatures (T_{eff}), sources obvious still actively accreting material or with mass outflow (e.g. ASR 1 has CO emission, ASR 114 has H_2 emission), and sources of pure line emission (e.g. ASR 57 has H_2 emission). Table 3 presented a qualitative classification of the spectral features of all 33 sources. We find that 15 sources have a rising red continuum while 10 sources have a continuum rising to the blue. Seven sources possess a relatively flat continuum over the wavelength range observed while one source (ASR 57) has no detectable continuum flux. Eight sources possess H I recombination line (Brγ 2.166μm) emission, while 1 source (ASR 130) shows Bγ in absorption. Eight sources show rovibrationally excited H_2 emission (in the form of the v=1-0 S(1) line at 2.122μm). In Na I (doublet, 2.208μm), 18 sources show absorption while one source (ASR 1 aka SSV13) shows emission and 13 sources show no Na I feature. In Ca I (triplet, 2.264μm), 22 sources show absorption while zero have this feature in emission. This means that 11 sources show no Ca I feature. In the molecular ^{12}CO bandhead at 2.294μm, 22 show CO absorption, one shows CO emission (again, ASR 1) and 10 show no feature. The conclusion reached, therefore, by a preliminary inspection of the 2μm spectra, in particular by the strength of CO, Na I and Ca I, is that the majority of sources superficially resemble cool low-mass dwarf stars.

3.1.2. H_2O

In addition to the aforementioned atomic and molecular features, H_2O has pronounced (>10% absorption wrt the local continuum) broad absorption features at ∼2μm and 2.5μm in dwarf stars of spectral types later than M0 V. In giants, H_2O absorption is weaker than in dwarfs of the same spectral classification (Aaronson et al. 1978) and only significant (at the aforementioned level) at spectral types later than M5 III. For sources on the ZAMS and background giants, using the presence (or non-detection) of H_2O as an indicator of spectral classification seems a reliable method of constraining the stellar T_{eff}. However, one point that remains unresolved is whether we should use the spectral type at which H_2O absorption becomes significant in l.c. III sources as the lower limit to the spectral type of over-luminous PMS dwarf showing l.c. III giant-like absorption. For example, for a PMS dwarf over-luminous wrt its final ZAMS spectral type and hence showing giant-like 2μm absorption features from a low surface gravity extended (hence over-luminous) atmosphere, can we utilize the presence of H_2O absorption to constrain the stellar spectral classification by using the giant spectral type at which H_2O absorption becomes significant as a lower limit even though the source is certainly a PMS dwarf? Since the variation in H_2O absorption (as well as metal and molecular absorption) with PMS age and mass has not been explicitly predicted by current PMS evolutionary models, it is likely that such a usage of H_2O as a diagnostic to spectral classification would be at best crude. Regardless of this however, we will use in subsequent analysis H_2O absorption as a secondary method of constraining spectral types when other data is also available. We note that such analysis may have to be modified at a later date when a better understanding of H_2O (etc) absorption in PMS objects is achieved.

In our spectra, H_2O absorption is likely best seen in continuum subtracted spectra where it will appear as broad 'dips' at the above wavelengths. However, in sources with significant CO absorption, the longer wavelength H_2O feature is masked by the higher transitions of CO suggesting that the shorter wavelength feature would be the best diagnostic of spectral type. As we shall see below (Section 3.9, Appendix A), H_2O is readily detected in cool, low-mass stars at 2μm with the resolution achieved here.

3.2. Source photometry

In Fig. 4 we show the JHK c-c (left) and K vs. H-K colour-magnitude (KHK c-m, right) diagrams for the sources we have observed spectroscopically. These data are taken from Paper I.

In the JHK c-c diagram, the sources for which we have spectra cluster around the loci of the reddened ZAMS/giant branch. Objects lying in this region, as opposed to those possessing obvious thermal NIR excess emission (e.g. ASR 114), are difficult to classify since they could be either reddened ZAMS stars or PMS stars e.g. classical T Tauri stars (CTTS). The locus of possible intrinsic unreddened weak line T Tauri (WTTS) and CTTS colours (from GM95) is shown by the dashed line. Clearly, sources located in the region defined by the lower ZAMS reddening vector and the reddening vector from the extreme CTTS colour (the dot-dashed line) can also suffer from the same discrimination problems. Ten sources observed lie outwith the bounds of reddened ZAMS/giant branch stars or the reddened CTTS region.

The KHK c-m diagram demonstrates the large range of source m_K values and H-K colours present in our spectroscopic sample. Plotted is the ZAMS locus for 318pc (solid line with open circles) and a reddening vector of A_V=7 magnitudes. This is the average A_V through the NGC 1333S cloud. Few sources lie close to the unreddened ZAMS implying either they are reddened by the associated molecular cloud (likely) and/or younger than the ZAMS as indicated by evolutionary tracks of D'Antona & Mazzitelli (1994, 1997) and shown, for example, in WGM99 Fig. 1. Both these possibilities are likely for the PMS objects in NGC 1333S.

3.3. The 2μm continuum flux

The spectra shown in Figs. 1 and 2 are, in many cases, composed of emission and absorption from three distinct physical processes, i) stellar photospheric emission/absorption, ii) thermal emission from heated dust in the circumstellar environment, and iii) reddening by overlying material both immediately surround the star (its circumstellar envelope) and in the intervening molecular cloud. Attempting to derive the relative contributions of these three processes is not a simple matter. In their NIR spectroscopic study of massive hot young stars, Porter et al. (1998) found that fitting the 1–1.5μm NIR emission flux with reddened stellar photospheric emission gave good definition of the intervening extinction. This assumed that the continuum emission seen in this passband is free from thermal emission components.

The values they derived were consistent with their secondary determination of extinction from NIR H I line ratios. A similar treatment of the observed 2–2.5μm flux in their sources often gave spurious results due to the present of significant thermal emission (see Porter et al. Fig.2). Since all their sources were massive hot stars, Porter et al. assumed an underlying 30000K stellar spectrum (stars with T_{eff} >30000K show similar continuum emission over this wavelength since the Rayleigh-Jeans tail is being observed) which was reddened to match the observed 1–1.5μm continuum emission. Since here we have only 2–2.5μm spectra (likely often containing a thermal emission component) and we cannot make the assumption that the underlying stellar photosphere is similar in all sources (we could be observing stellar photospheres with temperatures anywhere in the range [brown dwarfs] 1500K<$T_{eff} < 30000K$ [high-mass stars]) we clearly cannot use the same approach. To add to the complexity of continuum determination, Jones et al. (1996) demonstrated that for cool M dwarf stars the derivation of a stellar T_{eff} can be effected by the present of the aforementioned broad water vapour (H_2O) bands which can mask the true stellar continuum level and shape. In the 2–2.5μm window, broad H_2O bands are seen at ~2μm and 2.5μm, e.g. at each end of the K-band spectra range, in cool dwarf and giant stars. Consideration of the 2μm spectrum of the brown dwarf Kelu-1 (Ruiz et al. 1997), candidate brown dwarfs in ρ Oph (WGM99), standard main sequence stars (Ali et al. 1995), and high-mass young stars (Porter et al. 1998) suggests that the wavelength range 2.15–2.3μm could be used for continuum definition since it is relatively free from H_2O absorption and contain only narrow spectral features such as Brγ, Na I, Ca I, and weak H_2 emission lines. Consideration of this wavelength range as a continuum definition region will allow us to assess whether our sources can be represented by reddened photospheric emission alone or contain a thermal emission component. In addition, subtracting a continuum defined in this manner will allow us to better observe any H_2O absorption at 2μm giving an additional diagnostic of spectral type. Before presenting this analysis however, we first consider the effect of extinction and thermal emission on the shape of NIR stellar continuum emission since this is critical to the correct definition of the underlying stellar continuum flux and associated T_{eff}.

3.4. The effect of extinction

An interesting presentation of the effect of overlying extinction on a stellar spectrum was given in Greene & Lada (1996). The observed spectrum of a low extinction (A_V <3) red star Gl 166c (M4.5V) was shown (see their Fig. 2) as observed and artificially reddened by A_V=5, 10, 20, 30 and 60 magnitudes. These plots show how the apparent spectrum of a source can be distorted by overlying extinction, in fact, distorted to such an extent that both major broad features like H_2O absorption and atomic absorption features like Na I and Ca I, easily detected in the observed spectrum, are hardly noticeable (in normalized spectra) at A_V=20 and above. As noted by Greene & Lada, the overall shape of YSOs spectra can generally be understood largely in terms of various amounts of reddening.

In Fig. 5 we present the results of numerical modelling of the effect of reddening on spectra dominated either by emission from heated dust (500K< T_{bb} <3000K) or stellar photospheric emission (3000K< T_{eff} <10000K). Such a demonstration has not been previously presented and we consider it a useful diagnostic in the interpretation of NIR young star spectra in embedded regions. For a range of A_V of 0–50 magnitudes (typical of stars observed in SFRs in the NIR), we have generated single-component emission (black-body, BB) spectra for the above range of temperatures. Each panel of Fig. 5 shows the results for one applied A_V value (0, 10, 20, 30, 40, 50 magnitudes, respectively). Close inspection show that over the relatively restricted wavelength range considered (2–2.5μm) a reddened stellar photosphere can look remarkable similar to a less reddened thermal emission spectrum. For example, a 10000K stellar photosphere with A_V=30 magnitudes (middle-right panel) looks very similar to 1000K thermal emission with A_V=0 (top-left panel). Hence, fitting the 2–2.5μm continuum with a single stellar photosphere model can clearly give results widely discrepant from reality. In Section 3.7 below we shall see how the the best-fit T_{eff} changes with increasing A_V for sources observed in NGC 1333S.

If we consider the added complication that any observed stellar spectrum could be composed of a fraction η of photospheric emission and (1-η) of thermal emission, plus subsequent reddening, the interpretation of the continuum slope becomes even more complex. Fig. 6 shows examples of such composite spectra. Here we show plots of model 2–2.5μm spectra with an increasing contribution from thermal emission (from 0 to 0.9) for each plot. The different plots show the same spectra (with the same ratios of thermal to photospheric emission) reddened by A_V=0 to 50 magnitudes again in steps of 10 magnitudes. A photospheric temperature of 4000K was chosen as being a typical low-mass PMS star temperature together with the fact that temperatures higher than ~3000K produce (unreddened) spectra of very similar slope over the 2–2.5μm wavelength range considered here (see Fig. 5 top-left) since (as in the high-mass stars spectra of Porter et al.) we observe the Rayleigh-Jeans tail of the emission function. The plots in Fig. 6 show clearly that above A_V~20 even pure 4000K photospheric emission (η=1) rises to the red suggesting the presence of a cooler thermal emission component. For unreddened (A_V=0) emission, above about η=0.5 i.e. 50% photospheric emission and 50% thermal emission, the observed spectrum also rises to the red.

3.5. Fitting the stellar continuum

We next subtract a 'continuum' component from the NGC 1333S source spectra defined by fitting the observed spectra, over the wavelength range 2.15-2.3μm (see above) with single component model BB emission spectra in many cases including the effect of overlying extinction. For sources with CwR=Y from Paper I, and hence with a derived A_V value (from dereddening them onto the ZAMS in a JHK c-c diagram), we have used this value to reddened the model spectra before fitting to the observations. The results of the continuum definition by this method are shown in Table 3 while the continuum subtracted source spectra are shown in Fig. 7.

Using T_{eff} values for specific spectral types for ZAMS dwarfs and giants stars (cf. 'Astrophysical Quantities') we can compare the best-fit temperatures, T_{der} in Table 3 with the T_{eff} values from their implied spectral types (spectral types from Paper I, also shown here in Table 1) using the estimated A_V values from dereddening onto the ZAMS in the JHK c-c diagram shown in Fig. 4. If good correlation is found we gain support for the interpretation of the source as being reddened background stars with CwR=Y. Alternatively, if poor correlation is found then the continuum over the fitted wavelength range is either not well represented by reddened single temperature black-body emission or the assumed A_V is incorrect. The T_{eff} for each source, using the implied spectral types from Paper I (shown in Table 1 column 6) are given in Table 3 column 8.

Of the 33 sources observed, 17 have CwR=Y while 7 others have colours that lie either close above (C_A) or close below (C_B) the reddened ZAMS. Hence, 24 sources have implied A_V values/spectral types from Paper I. Of these only 3 (ASR56, 123 and 130) have implied T_{eff} values within ±1000K of the temperatures of the best-fit continua assuming the implied A_V values. The majority of sources have T_{der} values considerably smaller than the implied T_{eff} values. Of the remaining 21 sources, 9 (ASR 8, 24, 37, 43, 51, 106, 115, 120, and 121) have implied T_{eff} from dereddening of >10000K (6 of these have implied T_{eff} >20000K) and are hence all sources with implied spectral types earlier than A0 V (B3 V). The spectral features seen in all of these sources imply a spectral classification considerably later than A0 V since all 9 sources have NIR CO absorption, 6 have Na I absorption and 7 have Ca I absorption. Of the 9 sources, 6 have T_{der} ≤2,500K, 2 have T_{der} ~3000K and 1 has T_{der} ~5000K. The 2μm spectra of the majority of these sources therefore must be effected by thermal circumstellar emission rather than dominated by photospheric emission. The one source with T_{der} ~5000K, ASR120, also possesses Brγ emission implying the presence of a source of ionizing radiation in addition to a cool component.

The remaining 12 sources (from the sub-set of 21) all have implied T_{eff} values in <10000K with a maximum of 8000K (ASR44) and a minimum of 3400K (ASR40). Their corresponding T_{der} values range from 2500K to 1400K. These values suggest that the NIR spectra of these sources are dominated by thermal emission or the implied (from dereddening) A_V values are incorrect. Of these 12 sources all show CO absorption (although in ASR112 it is very weak), 10 show Na I absorption (weak in 6 sources) and 10 show Ca I absorption (weak in 6 sources, the same 6 as the weak Na I absorption). One source shows weak Brγ emission (ASR122) while the other sources show neither Brγ emission nor absorption. The presence of CO absorption in all the spectra implies a spectral type later than late-G V (or mid-G-III) with T_{eff} <5,300K. This means that the earlier (than late-G V) spectral types from dereddening implied for ASR44 (8000K), ASR86 (7,200K), ASR125 (5,800K) and ASR128 (5,500K) are all erroneous.

3.6. The multiplicity of best-fit models

From what we have found regarding the multiplicity of 'best fit' models to NIR continuum emission (in Section 3.5), it it clear that several such models with different combinations of T_{der} and A_V will equally well fit the data. Fig. 8 shows examples of such multiplicity for the sources ASR 8 and ASR 40. In this plot the best fit A_V value and corresponding T_{der} values are shown for both sources. All models with parameters lying along these curves fit the observed 2.15–2.3μm continuum equally well. We note from these two representative plots that as the best-fit temperature increases so does the best-fit A_V value (due to the reddening nature of extinction). In the regime of thermal circumstellar emission (<3000K) the best-fit is highly sensitive to the determined A_V values. In the regime of photospheric emission (>3000K) the best-fit is sensitive to temperature rather than A_V (which is large and insensitive to the best-fit T_{eff}). In the case of ASR40 (see Fig.8) using the A_V value implied by dereddening onto the ZAMS in the JHK c-c diagram (i.e. 15 magnitudes) results in a low best-fit T_{eff} of ~1,500K. To enter the regime of photospheric emission (~3000K) would require increasing the A_V to 25 magnitudes and is inconsistent with its location in the NIR c-c diagram (see Fig.4). This would be the case for all the sources located between, or close to, the reddening lines from the ZAMS/giant branch implying that constraints can be placed on the best-fit model multiplicity.

3.7. Background giant density

In Paper I we used the Wainscoat et al. (1992, henceforth WGM92) galaxy model to predict the population of foreground and background stars we might expect in the NGC 1333S field. The results of the model were reddened, in a Monte-Carlo simulation of the NGC 1333S field extinction, and compared to the observed stellar population. This allowed the derivation of an intrinsic K luminosity function for the embedded PMS stars. The WGM92 model produced the expected population of stars of different spectral classification from five galactic stellar components i.e. disk, bulge, arms, ring and halo. Once these are combined, the total expected population of reddened background stars in the NGC 1333S field through the whole galaxy at this location (l=88deg, b=-20deg) can be estimated. This is very useful to our analysis here since in Paper I some of the stars (observed spectroscopically here) were classified as possible background giants and hence, knowledge of the expected number of such sources allows us to estimate the likelihood that a source is a reddened background giant or an embedded PMS dwarf.

To an m_K of 13, the faintest source observed spectroscopically here, the WGM92 galaxy model predicts that we should see a total of 21 stars in an unreddened $10'' \times 10''$ field (the field observed photometrically in Paper I). Of these 13 stars, only two are expected to be giants and both of these in the spectral type range K0-1 III. If we additionally consider molecular cloud extinction with an $\overline{A_V}$=7 magnitudes and hence an $\overline{A_K}$ ~0.7 (assuming Rieke & Lebofsky (1985) reddening), the number of (reddened) background stars seen at K declines to 6 but still includes the two K0-1 III giants. Table 4 summarises the predicted stellar population in the NGC 1333S field including the estimated background source distances since the population is dependent on galactic component be it disk, bulge, halo, etc.

3.8. Atomic and molecular spectral indices

The work of Kleinmann & Hall (1986, KH86) demonstrated that a good correlations exists between the strengths of atomic and molecular spectral features over the 2–2.5μm wavelength range and the luminosity class and T_{eff} of the star. This they illustrated in their Fig. 7 where a combined atomic index (defined as the sum of the integrated absorption in the Na I doublet at 2.208μm and the Ca I triplet at 2.264μm minus the H recombination absorption in the form of Brγ at 2.166μm) was plotted against the a molecular index (defined as the strength of the 2.296μm ^{12}CO (2–0) absorption). From such a diagram it is possible to distinguish between MS dwarf stars (luminosity class [l.c.] V) and giant branch stars (l.c. III). The range of spectral types observed was G3 V–M5.8 V and F8 III–M7 III corresponding to photospheric temperatures of 2,950K$<$T$_{eff}$ $<$5,800K. GM95 plotted a similar diagram using slightly different indices (the atomic index was Na I+Ca I and the molecular index the sum of the ^{12}CO v=2–0 and v=4–2 bands). Their Fig. 3 contains the loci of l.c. V and l.c. III stars together with their sample of young PMS stars in the ρ Oph molecular cloud. Distinguishing between l.c. V and III sources is important since it determines the physical location of the absorption process i.e. for sources of known distance and brightness inconsistent with them being giant stars, a location displaced from the l.c. V locus in a atomic index vs. molecular index plot implies absorption in a low surface gravity environment (like a giant atmosphere) rather than in a dwarf-like high surface gravity atmosphere. A low surface gravity could also be found around circumstellar accretion disks in PMS system. In the GM95 plot, all there target stars lay between the l.c. V and l.c. III loci implying intermediate stellar surface gravities and a PMS evolutionary nature (source discrimination was simplified in GM95 since the region of ρ Oph studied was selected because of the A$_V$ $>$50 of this region).

In order to apply the above analysis to the NGC 1333S sources, we first must consider whether spectral data at the resolution achieved here will produce the same correlation as in KH86 and GM95. The KH86 spectra are of considerably higher spectral resolution (R$\sim$25000) than our data (R$\sim$1000). We have therefore degraded the KH86 spectra to match the resolution of our targets by binning (a factor $\times$25) and smoothing (using a triangular filter of width 5 pixels). The resultant KH86 spectra are shown in Fig. 9. In recreating the atomic vs. molecular indices from these reduced resolution spectra we have used local continuum levels on each side of the spectral feature rather than the spectrally distant continuum emission bands used in KH86. We believe this results in improved determinations of the feature strengths, an important fact for lower signal:noise spectra (our sources have an average m$_K$ $\sim$9 magnitudes fainter than the KH86 sources). Fig. 9 shows the band passes where spectral indices have been calculated. In Fig. 10 we present our re-creation of the KH86 correlation plot for data extracted from the reduced resolution spectra. Since our spectra are of poorer quality than those in KH86 and almost all the stars observed in NGC 1333S have CO absorption (see Table 3) and only a few show Brγ (in emission or absorption), we use an atomic index of Na I+Ca I plotted against a molecular index of v=2-0 ^{12}CO.

It is clear that a strong relationship between atomic and molecular indices is present in Fig. 10 implying that the reduction in spectral resolution of the KH86 sources has not masked the intrinsic correlation. Comparison to the atomic vs. molecular indices plot for main sequence stars and PMS objects in Greene & Lada (1996, Fig 7) shows that for data at approximately the same spectral resolutions, the index values obtained are very similar. To demonstrate that this relationship is independent of extinction, we reddened the KH86 spectra by 10 and 20 magnitudes and re-calculated the atomic and molecular indices. The resultant plots for reddened stars showed no obvious differences from the un-reddened plot shown in Fig. 10 implying that this is a reddening independent correlation.

We have derived the modified KH86 atomic and molecular indices from our 2μm spectra of the NGC 1333S sources. The values obtained from the spectra are given in Table 5 and shown graphically in Fig. 11. The plot on the left shows the total range of atomic and molecular indices for the ASR sources while the plot on the right shows a closer view of the region containing the majority of sources. The uncertainties in the indices, due to intrinsic noise in the spectra and continuum definition errors, are estimate to be $\sim$ $\pm$0.5–1.0 in both the atomic and molecular indices for large to small indices values. Fig. 11 shows that the majority of objects are displaced from the l.c. V locus. The main physical property determining the location of a star in Fig. 11 is the surface gravity of the absorption region producing the atomic and molecular absorption features. PMS dwarf stars appear over-luminous wrt their eventual ZAMS spectral classifications (see tracks in Fig. 12). Since this is directly related to their emission surface area, over-luminous PMS stars with larger, lower gravity photospheres should appear more similar to giants in terms of their atomic/molecular absorption characteristics. Additionally, accretion disks around PMS stars can possess low surface gravity envelopes which could mimic giant atmospheres. Both these facts would significantly modify the location of PMS stars in Fig. 11. The two dotted lines joining the l.c. V and l.c. III loci are for stars of the same spectral types, K0 and K5–M2 (the indices for stars of spectral types K5–M2 in KH86 are similar and hence the upper dotted line represents the average indices for these stars). In the analysis below, we consider that PMS stars evolve along such (dotted) tracks as they contract towards the ZAMS with (to first order) constant surface temperature (at least at sub-solar masses). A consequence of this evolution is that the NIR CO bands decrease in strength significantly with age while there is only a correspondingly small change in the atomic line (Na I, Ca I) strengths.

From the above discussion, we conclude that when sources are considered spectroscopically in relation to other data e.g. NIR photometry and colours, the evolutionary state of these stars can often be determined. From Fig. 11 we can see that the NGC 1333S sources possess a large range of atomic and molecular indices. To obtain information on the intrinsic spectral types of the stars from this data requires a detailed analysis of their spectral indices and photometric properties. Appendix A presents this analysis for each source observed. To within the associated uncertainties, 9 sources (ASR2, 36, 51, 56, 106, 113 120, 122 and 123) have spectral indices shown in Fig. 11 that are consistent with dwarf (l.c. V) ZAMS stars or giants (l.c. III, only ASR56) values. However, the analysis in Appendix A suggests that only 3 of these sources (ASR2, 51 and 56) are true reddened background stars not in a PMS evolutionary state and not associated with the NGC 1333S SFR. This fact is consistent with the predictions of the WGM92 galaxy model. Of the other sources, 22 (ASR7, 8, 37, 40, 42, 43, 44, 46, 78, 86, 105, 106, 107, 111, 112, 114, 118, 121, 125, 128 and 130) have indices indicative of absorption in giant-like low surface gravity atmospheres however, ASR130 is likely a reddened background star (see Appendix A). Finally, two sources (ASR1 and 57) lie to the left of the l.c. V locus in Fig. 11 implying they have significant atomic absorption but little molecular absorption. One source (ASR57) shows no continuum emission and only H_2 line emission while one other source (ASR1) shows CO, Ca I and Na I in emission.

Table 6 presents the conclusions drawn as to the nature and spectral types of the stars in our spectroscopic sample from the atomic vs. molecular indices plot. Of the sample of 32 stellar sources (ASR57 is a region of shock-excited H_2 emission and not included in the statistics here), only 4 are found to be reddened background stars. The majority (28) are classified as PMS stars in the NGC 1333S PMS cluster from their spectroscopic characteristics. This result confirms the conclusions drawn in Paper I since all stars classified as PMS photometrically are designated PMS stars spectroscopically also. Seven sources either classified as reddened background stars (4) or stars with undetermined classifications (3) in Paper I are found to be PMS stars here spectroscopically. Additionally, spectral types considered accurate to ±1 spectral type sub-classes are determined for 26 of the 32 (stellar) source. Two other sources have classifications accurate to ±2 sub-classes while four others have undetermined spectral types. Of the 26 stars with reasonably good determinations of spectral types, 13 are classified early- to mid-M V, 3 mid- to late-K V, 6 early- to mid-K V, 2 early- to late-G V, 1 early-A V and 1 early-K III meaning that the majority (22) are later spectral type than the Sun and are hence, of sub-solar mass.

4. The H-R diagram for the NGC 1333S PMS stars

The aim of the above analysis is to both clarify the evolutionary state of the objects observed and obtain estimates of their masses and ages. Specifically, we have used 2μm spectroscopy together with earlier NIR photometry to determine which stars in the sample are PMS objects. We now use the spectral type and absolute K magnitudes (M_K) obtained to place these objects on the Hertzsprung-Russell (H-R) Log $L/L_\odot$ vs. Log T_{eff} diagram. To do this however, we have to convert both the spectral types into T_{eff} values and the M_K values into luminosities. There have been several such analyses published recently e.g. WGM92, Carpenter et al. 1997) and we have here used the compilation of spectral types vs. T_{eff}, visual bolometric corrections (BC_V), and optical to NIR colours of Kenyon & Hartmann (1995, KH95). Their Table A5 quantifies these parameters for main sequence stars of spectral types B0 V to M6 V. The procedure followed was to use the V-K source colour from KH95 to give M_V then apply the appropriate BC_V to obtain source M_{bol}. These values were next converted to luminosity (in $L_\odot$) using the relationship

$$Log\ L/L_\odot \ = \ -(M_{bol} \ - \ M_{bol\odot})/2.5 \qquad (1)$$

assuming $M_{bol\odot}$=4.72. We hence obtain the values for for luminosity and T_{eff} shown in Table 7. Also given are the estimated source M_{bol} values. Most sources listed in Tables 6 and 7 have spectral types accurate to a 1-2 classification sub-classes and the T_{eff} values used are for the centre of the estimated range of spectral types and should be accurate to $\pm$400K.

Fig. 12 shows the H-R diagram for these sources overlaid on PMS evolutionary tracks (for masses 0.16$M_\odot$ to 2$M_\odot$) and isochrones (from age 7×10^4 years to 5×10^8 years) from D'Antona & Mazzitelli (1997)[3]. The inherent uncertainty in T_{eff} and luminosity are demonstrated by the representative error bar at the bottom-left corner. Only stars with reasonably good determinations of spectral types from the above analysis are included i.e. those with spectral types determined to within $\pm$1 sub-classes. These 26 sources are shown in Fig. 12 and range in luminosity from $\sim$0.007$L_\odot$ (ASR2) to $\sim$7$L_\odot$ (ASR120) and T_{eff} from $\sim$3370K (ASR24,37) to $\sim$5520K (ASR7). ASR130 is not shown in Fig. 12, even though it has a well-determined spectral type, since it is close to the ZAMS and has a T_{eff} considerably to the left of the rest of the sources.

From Fig. 12 we can estimate masses and ages by comparison with the PMS evolutionary tracks. However, as noted by D'Antona & Mazzitelli, these tracks should only be used as rough guides to the physical properties of observed sources. In Table 8, therefore, we present masses and ages for the NGC 1333S sources and note they should be treated with a certain degree of caution. With this in mind, we note that there appears to be a significant range of source ages in NGC 1333S from relatively young PMS objects with ages of 7×10^4 years (e.g. ASR42, 128) to older sources close to, and in some cases on, the ZAMS at 1×10^8 years (e.g. ASR8 , 130). This is consistent with previous observations (discussed in Section 1) whereby young Class 0/I sources still actively producing outflows are seen together with more evolved (Class II) PMS objects. The majority of the sources span the mass range covering low-mass T Tauri star i.e. 0.2–1.5$M_\odot$.

With a larger sample of stars covering the complete brightness range of sources found in NGC 1333S (see Paper I) it would be highly informative to present a diagram of the number of sources per mass range vs. mass to study the initial mass function of the region. However, with only 33 sources out of the total observed photometrically at K (134) plus our sampling of the brighter end of the luminosity function of the region, we feel that such a plot would not be meaningful. All we can say is that, according to our analysis and Fig. 12, there is a significant population of both low-mass (M$\leq$0.5$M_\odot$) and low- to intermediate-mass (0.5$\geq$ M $\leq$1.5$M_\odot$) in the region. In addition, with a more complete sample of stars we could investigate the spatial segregation of sources with age and determine if PMS in the same general location are of similar ages or otherwise.

5. Conclusions

We have obtained 2μm spectra of a sub-sample of 33 sources in the NGC 1333S SFR which at K possesses a total of 134 sources. The aims of this work are to both refine the membership of the PMS stellar cluster and to study the physical characteristics of the individual sources in more details. Of the 33 sources, we have demonstrated that 29 are found to be young stars associated with the NGC 1333S cluster. From the spectral features we have derived spectral classifications and hence T_{eff} and M_{bol} values from which we have placed 26 of the sources on the H-R diagram. Comparison with PMS evolutionary tracks and isochrones suggests that for the optical and NIR sources there exists a significant range of stellar ages within the region from embedded Class I sources of less than 1×10^5 years of age to to more evolved sources close

[3]The PMS tracks and isochrones of D'Antona and Mazzitelli are available from F. D'Antona on the www at URL http://mporzio.astro.ir/d̃antona.

to becoming ZAMS stars of ages up to $\sim5\times10^7$ years. The mass range sampled by our survey is $\sim$0.2–2$M_\odot$and hence we have observed objects from the population of low- to intermediate-mass objects.

Further progress on the cluster membership determination and the spectral classification of sources can certainly be made. Clearly extending the sample to include fainter objects, and hence observing more thoroughly the mass regimes of low-mass stars ($<0.3M_\odot$) to very low-mass stars ($<0.2M_\odot$) to brown dwarfs (BDs, $<0.08M_\odot$), is important. At 318pc (distance modulus of 7.5), a BD of mass $0.08M_\odot$ and age 7×10^6 years would have $L\sim0.01L_\odot$ and (using the data of WGM99 cf. their Table 5) an M_{bol} $\sim$9.7 and (spectral type of M9 V and BC_K=3.2) an M_K $\sim$6.5 and an m_K $\sim$14.0. On the ZAMS, such a BD would have $L\sim0.001L_\odot$, M_{bol} $\sim$11.4, M_K $\sim$8.2 and m_K $\sim$16.5. Thus, in NGC 1333S, unreddened young BDs would be relatively easy to observe spectroscopically (as opposed to BDs on the ZAMS) as demonstrated in ρ Oph by WGM99. By extending the spectroscopic sample by $\sim$3 magnitudes therefore, we can observe stars to below the H-burning limit and produce a true initial mass function for the PMS cluster. In addition, extending the observing to other wavelength regimes to obtain improved spectral classifications (V, R for optically visible sources, H and J NIR bands for NIR sources, 10μm for more embedded and younger Class I sources) is clearly valuable. As we have seen above however, using 2μm spectra alone does pose some problems which the addition of data at one other wavelength could answer.

Finally, it is clear that the addition of spectroscopic data to photometry is extremely important to make progress in understanding the star formation process for individual sources and clusters of stars by allowing the derivation of more reliable spectral types and hence T_{eff} values and source masses and ages. Using multi-object spectroscopic (MOS) techniques in the NIR would greatly enhance the data quality achieved by its simultaneity and improve the statistical properties of datasets by allowing larger number of objects to be easily observed.

We wish to acknowledge the Panel for Allocation of Telescope Time for the observing time during which the data presented above were acquired. We also thank T. Greene, M. Meyer and N. Calvet for useful discussions, F. D'Antona for information on PMS evolutionary model tracks/isochrones and the conversion of M_K and spectral types to luminosity and T_{eff}, and R. Wainscoat for providing results from his galaxy model for the original work on NGC 1333S in Paper I. The United Kingdom Infrared Telescope is operated by the Joint Astronomy Centre on behalf of the U.K. Particle Physics and Astronomy Research Council (PPARC). We thank the staff of UKIRT for their support during the acquisition of these data. This work was supported by the Gemini Observatory, which is operated by the Association of Universities for Research in Astronomy, Inc., on behalf of the international Gemini partnership of Argentina, Australia, Brazil, Canada, Chile, the United Kingdom, and the United States of America.

REFERENCES

Ali B., Carr J.S., Depoy D.L., Frogel J.A., Sellgren K., 1995, AJ, 110, 2415

Aaronson M., Frogel J.A., Persson S.E., ApJ, 220, 442

Aspin C., Sandell G., Russell A.P.G., 1994a, A&ASup, 106, 165 (ASR, Paper I)

Aspin C., Reipurth B., Lehmann T., 1994b, A&A, 288, 165

Aspin C., Sandell G., 1997, MNRAS, 289, 1 (Paper II)

Aspin C., Greene T., Reipurth B., 2000, in prep.

Bachiller R., Cernicharo J., 1986, A&A, 166, 283

Biscaya A.M., Rieke G.H., Narayanan G., Luhman K.L., Young E.T., 1997, ApJ, 491, 359

Blake, G.A., Sandell G., Van Dishoeck E.F., Groesbeck T.D., Mundy L.G., Aspin C., 1995, ApJ, 442, 694

Carpenter J., Meyer M.R., Dougados C., Strom S.E., Hillenbrand L.A., 1997, AJ, 114, 198

Casali M.M., Matthews H.E., 1992, MNRAS, 258, 399

Černis K., 1990, Astron. Space Sci., 166, 315

D'Antona F., Mazzitelli I., 1994, ApJSup, 90, 467

D'Antona F., Mazzitelli I., 1997, Mem. Soc. Astron. It., 68, 4

de Zeeuw P.T. et al., 1999, AJ, 117, 354

Eiroa C., Casali M.M., 1992, A&A, 262, 468

Greene T.P., Meyer M.R., 1995, ApJ, 450, 233 (GM95)

Greene T.P., Lada C.J., 1996, AJ, 112, 2184

Harvey P.M., Wilking B.A., Joy M., 1984, ApJ, 278, 156

Herbig G.H., 1974, Lick Obs. Bull. No. 658

Herbig G.H., Bell K.R., 1988, Lick Obs. Bull. No. 1111

Herbig G.H., Rao N.K., 1972, ApJ, 174, 401

Herbig G.H., Jones B.F., 1983, AJ, 88, 1040

Hodapp, K-W., Ladd E.F., 1995, ApJ, 453, 715

Jennings R.E., Cameron D.H.M., Cudlip W., Hirst C.J., 1987, MNRAS, 226, 461

Jones H.R.A., Longmore A.J., Allard F., Hauschildt P.H., 1996, MNRAS, 280, 77

Kenyon S.J., Calvet N., Hartmann L., 1993, ApJ, 414, 676

Kenyon S.J., Hartmann L., 1995, ApJSup, 101, 117

Kleinmann S.G., Hall D.N.B., 1986, ApJSup, 62, 501 (KH86)

Koornneef J., 1983, A&A, 128, 84

Lada C.J., Depoy D.L., Merrill K.M., Gatley I., 1991a, ApJ, 3714, 533

Lada, E.A., Evans, N.J. II, Depoy, D.L., Gatley, I., 1991b, ApJ, 371, 171

Lada C.J., Adams F.C., 1992, ApJ, 393, 278

Lada C.J., Alves J., Lada E.A., 1996, AJ, 111, 1964 (LAL96)

Ladd E.F., Lada E.A., Myers P.C., 1993, ApJ, 410, 168

Ladd E.F., Myers, P.C., Goodman A.A., 1994, ApJ, 433, 117

Langer W.D., Castets A., Lefloch B., 1996, ApJLet, 471, L111

Liseau R., Sandell G., Knee L.B.G., 1988, A&A, 192, 153

Luhman K.L., Rieke G.H., Lada C.J., Lada E.A., 1998, ApJ, 508, 347

Meyer M.R., 1996, Ph.D. thesis, University of Massachusetts, Amherst, Jan 96.

Mountain C.M., Robertson D., Lee T.J., Wade R., 1990, SPIE, 1235, 25

Porter J.M., Drew J.E., Lumsden S.L., 1998, A&A, 332, 999

Puxley P.J., Beard S.M., Ramsay S.K., 1992, Proc. of the ESO/STECF 4th Data Analysis Workshop, Garching.

Rieke G.H., Lebofsky M.J., 1985, ApJ, 288, 618 (RL85)

Ruiz M.T., Leggett S.K., Allard F., 1997, ApJ, L107

Sargent A.I., 1979, ApJ, 233, 181

Sandell G., Aspin C., Duncan W.D., Russell A.P.G., Robson E.I., 1991, ApJ, 376, 17

Sandell G., Knee L.B.G., Aspin C., Robson E.I., Russell A.P.G., 1994, A&A, 285, 1

Sandell G., Knee L.B.G., 1998, in prep.

Sato S., Nagata T., Tanaka M., Yamamoto T., 1990, ApJ, 359, 192

Saraceno P., André P., Ceccarelli C., Griffin M., Molinari S., 1996, A&A, 309, 827

Strom S.E., Grasdalen G.L., Strom K.M., 1974, ApJ, 191, 111

Strom S.E., Vrba F.J., Strom K.M., 1976, AJ, 81, 314 (SSV)

Strom K.M., Strom S.E., Stocke J., 1983, ApJLet, 271, L23

Strom K.M., Strom S.E., Wolff S.E., et al., 1986, ApJSup, 62, 39

Strom K.M., Magulis M., Strom S.E., 1989, ApJ, 345, L79

Wainscoat R.J., Cohen M., Volk K., et al., 1992, ApJSup, 83, 111

Ward-Thompson D., Buckley H.D., Greaves J.S., Holland W.S., André P., 1996, MNRAS, 281, 53

Warin S., Castets A., Langer W.D., Wilson R.W., Pagani L., 1996, A&A, 306, 935

Wilking B.A., Greene T.P., Meyer M.R., 1999, AJ, 117, 469

This 2-column preprint was prepared with the AAS LaTeX macros v5.0.

A. Details on the interpretation of source spectral features

ASR1 (SSV13) shows little evidence on its underlying spectral classification from its NIR spectrum due to its emission nature. However, it is clearly a young PMS object still actively accreting with variability in CO emission being observed by Biscaya et al. (1997).

ASR2 lies close to the M4 V location on the l.c. V locus in Fig. 11 inconsistent with its dereddening classification from Paper I of K0-3 V (A_V=2 at 350pc). However, closer inspection of its location in the JHK c-c diagram shows that, within the errors, its colors (J-H=0.62, H-K=0.23) can be interpreted as it being a M3 V star with no significant reddening. This was not considered in Paper I since the location of ASR2 is slightly bluer than the cool M dwarf regime of the ZAMS. If ASR2 is a PMS star in the NGC 1333S molecular cloud with an M3-4 V spectral classification, it would be over-luminous by ∼4 magnitudes. If ASR2 is an unreddened M3-4 V ZAMS star it would be at a between us and the NGC 1333S molecular cloud (d∼50) explaining why it is not reddened. Since the 2μm spectrum of ASR2 and both its JHK (Paper I) and JKL colours (Paper II) suggest it to be an M3-4 V unreddened star, this seems the most likely explanation.

ASR7 (SSV14) has a large implied extinction (A_V ∼20 magnitudes) from dereddening onto the ZAMS (see Fig. 4) and a location in the JHK c-c diagram (in Paper I) consistent with a late-type (M3-6 III) giant star. In Paper I, it was noted to have a close stellar companion plus an associated nebulous component. In Paper II ASR7 was given a classification based on a JKL c-c diagram consistent with that from Paper I. The location of ASR7 in Fig. 11 implies a spectral type of late-G III (since the giant sequence dips below the displayed linear locus at these spectral types, see Fig. 10). With this classification, ASR7 should show stronger Brγ absorption (see Fig. 9 spectrum p) than Na I absorption. In our high signal:noise spectrum (ASR7 is bright at m_K=9.66) however, no Brγ absorption is observed. Its implied (extinction corrected) M_K is ∼0.7 (d=318pc) implying an early-A V classification i.e. inconsistent with the spectral features observed and its location in Fig. 11. If we assume the implied late-G III classification is correct then ASR7 would be at 650pc. The WGM92 galaxy model prediction (Table 5) is that there is little chance of there being a giant star of spectral type earlier than K0 III in the observed field and even these should be at d>3kpc resulting in m_K values >11. This makes the interpretation of ASR7 as a background giant improbable. The presence of H_2O absorption at 2μm (see Fig. 7), which for l.c. III sources should only be presence in sources of spectral type M5 III or later, supports this interpretation. If we assume ASR7 is a PMS dwarf in the NGC 1333S SFR at 318pc then it would best be interpreted as a late-G V star and ∼3.5 magnitudes over-luminous. A late-G V classification is consistent with the spectral type inferred from projecting the location of ASR7 back to the l.c. V locus (in Fig. 11) parallel to the dotted lines (of constant spectral classification). Any later spectral classification for ASR7 would result in a larger over-luminosity factor which would rapidly become unrealistic. Why ASR7 shows no Brγ absorption is unclear although actively accreting young PMS stars can emit in Brγ which may veil its underlying photospheric absorption. Also, why an over-luminous late-G V PMS star would show H_2O absorption as seem in ASR7 is problematic since, for l.c. V sources, H_2O absorption should not be present in stars of spectral type earlier than ∼M0 V. Reviewing the data we have on ASR7 suggests that the most likely interpretation of ASR7 is that it is an over-luminous (by ∼4 magnitudes) late-G dwarf in the NGC 1333S molecular cloud. However, further observational clarification is certainly required.

ASR8 is located at a position in Fig. 11 where K2-3 III stars are found (see Fig. 10). It has an implied spectral type from dereddening in the JHK c-c diagram of Paper I of O-B V since it lies on the reddened extreme of the ZAMS. However, its location in this plot is also close to the locus of unreddened T Tauri stars (see Fig. 4). The 2μm spectrum of ASR8 shows strong CO absorption but only weak absorption in both Na I and Ca I and with an m_K of 12.2 (assuming 318pc) its M_K is 4.7 (assuming no reddening onto the T Tauri locus) and ASR8 would be an K7-8 V (ZAMS) star. The fact that ASR8 resembles an early-K giant in Fig. 11 can only be explained by the presence of a low surface gravity atmosphere producing deep CO absorption. If ASR8 is a background K2-3 III, as its location in Fig. 11 suggests, it would have to be at a distance of ∼7kpc. The WGM92 galaxy model predicts a very low probability of a K2-3 III star being present in the NGC 1333S field. Thus, we conclude that ASR8 is likely a T Tauri star associated with the NGC 1333S SFR. Projecting the location of ASR8 in Fig. 11 towards the l.c. V locus i.e. parallel to the dotted spectral type loci, gives a spectral classification of early-K V. However, to within the errors (ASR8 is at the fainter end of our spectroscopic sample), ASR8 could be a classified anywhere from an early-K V to early-M V star since (in KH86) dwarfs of spectral types K5 V to M2 V possess similar atomic and molecular indices (see above and Fig. 10). If ASR8 is an early-K V at 318pc its M_K would be 4.7 i.e. over-luminous wrt the ZAMS by ∼0.6 magnitude. Since ASR8 possess a giant-like atmosphere, which in turn implies it is an over-luminous PMS star, this is a reasonable conclusion. No strong H_2O absorption (at ∼2μm) is not surprising at this spectral type. We conclude that ASR8 is most likely an over-luminous early-K V PMS star within the NGC 1333S cluster.

ASR24 is located close to the l.c. I locus in Fig. 11 since it possesses deep CO bands and little to no Na I and Ca I absorption. Its spectrum is a little noisy (it is the faintest source in our spectroscopic survey) but the CO bands are nonetheless well detected. In the JHK c-c diagram of Paper I (Fig. 4 here), ASR24 is close to the intersect of the reddening vector from the high-mass end of the ZAMS and the T Tauri star locus implying, since it possesses CO absorption, it is likely a relatively unreddened PMS T Tauri-like star and not an mid-B V star as suggested in Paper I. Supporting this, the WGM92 galaxy model predictions imply we would not find a mid-B V star within the NGC 1333S survey field. In addition, its spectral features are indicative of a l.c. I supergiant also unlikely to be found in the survey field. ASR24 has an m_K of 12.9 and if located at 318pc would have an M_K of $\sim$5.4 corresponding to an M0-1 V ZAMS star. Why ASR24 shows no Na I and Ca I absorption (which should be strong in a early-M V ZAMS star) is certainly related to the fact that it is young and over-luminous and current possesses a very extended supergiant-like atmosphere. Its location in Fig. 11 is similar to that of known young FU Orionis (FUors) type low-mass outburst sources which generally show strong CO absorption and little to no atomic absorption (cf. Greene & Lada 1996 Fig. 7; Aspin, Greene & Reipurth, 2000). In FUors the low surface gravity absorption features are generally postulated to originate in the atmosphere of a massive disk (cf. Reipurth & Aspin 1997). There is some (albeit noisy) indication of H_2O absorption at 2μm but what this means for a PMS dwarf showing supergiant-like atomic and molecular absorption features is unclear. With the additional noise on its spectrum due to its relative faintness, it it possible that ASR24 is of a spectral type of mid-M V. At M3 V it would be up to 1.5 magnitude over luminous for its spectral type consistent with it showing low surface gravity atmospheric absorption. At M4 V ASR24 would be $\sim$3 magnitudes over-luminous. Such a classification is perhaps more consistent with the very low surface gravity supergiant-like atmospheric absorption clearly present in ASR24 suggesting it is a very young PMS star.

ASR36 lies above the cool end of the l.c. V locus in Fig. 11. Our spectrum of ASR36 is of somewhat lower signal:noise than those of other sources (see Fig. 7) and therefore the associated uncertainties in the atomic and molecular indices are likely larger than average. ASR36 is also designated SSS107 (Strom, Strom & Stocke 1993, SSS93) and is associated with wispy, arc-like Hα emission in optical images (see our R band image in Paper I Fig. 3a). An optical spectrum of the source by SSS93 showed a late-type ($\sim$M0 V) star reddened by $A_V \sim$2. Our Paper I classification (from a JHK c-c diagram) was a K3-6 V with $A_V \sim$2. This is consistent with the location of the source in our JKL c-c diagram in Paper II although exact spectral typing is difficult due to the similar colours for K-M V stars in these plots. ASR36 shows no thermal excess from J to L and in our 2μm spectrum shows no Brγ emission. The morphology of the associated Hα nebulosity suggests that it is originating from ASR36 however, it may possibly be a coincidental super-position and the Hα emission may be from, for example, Herbig-Haro emission objects which originates elsewhere. If ASR36 is a reddened K1-2 V main sequence star then its m_K of 11.4 places it at 275pc. If instead it is located in the NGC 1333S cloud (d=318pc) then it would be over-luminous for a K1-2 V with a M_K more typical of a late-G V. Its location in Fig. 11 is best interpreted as a late-type M4-5 V star which is inconsistent with both its optical spectroscopic classification and our (Papers I and II) photometric classifications. Such a star should have detectable H_2O absorption at 2μm since it shows dwarf-like absorption. ASR36 shows perhaps weak absorption (its spectrum is noisy at 2μm) suggesting it is at latest perhaps $\sim$M0 V. Since the optical spectrum of ASR36/SSS93 is clearly that of an M0 V and our 2μm spectrum is of relatively low signal:noise (with perhaps a spurious feature occurring on Na I, see Fig. 1), we must conclude that ASR36 is likely located in the NGC 1333S PMS cluster (due to its association with Hα emission) and is close to the ZAMS with an M0 V classification, little to no thermal excess, only moderately obscured and is over-luminous by $\sim$1 magnitude.

ASR37 has a 2μm spectrum possessing very little Na I and Ca I absorption (close to zero), but reasonably strong CO absorption (at 2.3μm) and H_2O absorption (at 2μm). In Paper I it was classified as a reddened (A_V=7) late-B V star which in the light of the 2μm spectral features observed, is incorrect. ASR37 lies in a similar location to ASR8 and 24 in the JHK c-c diagram (Fig. 4) i.e. close to both the unreddened T Tauri star locus and the reddening vector from the hot end of the ZAMS. It could also be classified as a slightly reddened (1-2 magnitudes) mid- to late-M V star by dereddening to the cool end of the ZAMS (instead of the hot end as in Paper I). In Paper II we found that the location of ASR37 in the JKL c-c diagram was consistent with that in the JHK c-c diagram (within the associated uncertainties). In Fig. 11 it is located close to the l.c. I source locus implying the presence of a very low surface gravity atmosphere. Its m_K (12.2) implies a unrealistic distance if it were a l.c. I source (also ruled out by the WGM92 galaxy model predictions, see Table 5) and we conclude it is a l.c. V source in the NGC 1333S cloud and hence a young PMS T Tauri star. The presence of H_2O absorption suggests a late-type spectral classification but relating this to dwarf stars when ASR37 shows supergiant-like atmospheric absorption is, as we have seen above, rather complex. At 318pc, its M_K would be $\sim$4.7 and indicative of a late-K V ZAMS stars. With its low surface gravity atmosphere, ASR37 is clearly an over-luminous young, PMS object and not on the ZAMS. If ASR37 is of spectral type M4 V star then it would be over-luminous by ∼3.5 magnitude and in a similar evolutionary state to ASR24, a source it is closeby in Fig. 11.

ASR40 is located between the l.c. V and l.c. III loci in Fig. 11. Its 2μm spectrum shows weak CO and Ca I absorption, and no Na I absorption. It also possesses H_2 emission in the form of a weak v=1-0 S(1) line at 2.122μm. In the JHK c-c diagram is lies on the reddened (A_V ∼15) cool end of the giant branch and was classified as a distant (d>3kpc) background M-type giant in Paper I. This interpretation is improbably from the predicted source counts in the WGM92 galaxy model (see Table 5). In the JKL c-c diagram (Paper II) ASR40 showed a 3μm thermal excess implying directly a PMS evolutionary state. At m_K=11.2, d=318pc and A_V ∼15, ASR40 would have an M_K ∼2.2 corresponding to a ZAMS star of classification ∼F4 V. Such a star would not possess CO absorption although with the low surface gravity absorption and a 3μm thermal excess, a disk origin for the CO is possible. However, disk CO, as in FUors with massive eruptive disks, generally places such sources in the l.c. I regime of Fig. 11 (see Aspin, Greene & Reipurth 2000) and not in the intermediate l.c. V–III zone. The latest spectral type ASR40 could be to produce a spectrum without significant Na I absorption is ∼K0 V (see Fig. 9). ASR40 is therefore likely a PMS T Tauri star with spectral type between late-F V and K0 V implying an over-luminous nature of ≤2 magnitude. Projecting its location in Fig. 11 to the l.c. V locus (parallel to the dotted lines) give a spectral type of more like K0-2 V (considering the associated uncertainties) reasonably consistent with the above determination. If ASR40 is a K0 V star it would be ∼2 magnitude over-luminous consistent with its intermediate surface gravity spectral features. The presence of H_2 emission directly on ASR40 without obvious extended nebulosity around the source or even nearby (plus no indication of H_2 emission from the other sources close to it e.g. on ASR120, ASR122, ASR36) implies that it is currently active and perhaps possessing outflow activity.

ASR42 (SSV18a) appears near the K2 III location on the giant locus in Fig 11. Its spectrum shows deep CO and weak Na I and Ca I absorption. In Paper I is was classified as a PMS star based on a dereddened spectral type of G6-9 V with A_V=6 at a distance of 275pc i.e. reddened but closer than the NGC 1333S molecular cloud when the cloud distance was thought to be 318pc. Since we have subsequently revised our working distance to NGC 1333S to 318pc (see above), its m_K of 11.6, would give a reddening corrected M_K ∼3.5 at 318pc and would be classified as a G5 V ZAMS star. The spectrum of ASR42 however, is not consistent with that of a G5 V ZAMS star (see Fig. 11) but more so with a K2 III which would then have to be at a distance of 3.7kpc. Such giants are scarce with the WGM92 galaxy model predicting a low probability that one is presence in the NGC 1333S field. A more acceptable interpretation is that ASR42 is a PMS object in the NGC 1333S cloud with absorption arising in a low surface gravity atmosphere (since ASR42 shows no thermal excess emission in either the JHK nor JKL c-c diagrams of Papers I and II we rule out a disk origin to the low surface gravity absorption features). Projecting its location in Fig. 11 back to the l.c. V locus, parallel to the dotted lines, suggests that ASR42 is an early- to mid-K V. The presence of low surface gravity absorption features imply it should be over-luminous for its classification which would have to be later than early-K V (to see such absorption at all). There is some indication of 2μm H_2O absorption in the spectrum of ASR42 (see Fig. 7) suggesting that, if ASR42 was an l.c. V star, it would be of spectral type at least early-M V. However, since ASR42 shows l.c. III giant-like absorption features, and giants have been shown to possess less H_2O absorption than the equivalent l.c. V spectral type (Aaronson et al. 1972), we cannot use the presence of H_2O to limit its spectral classification (especially in light of our discussion in Sect. 3.2.2). If ASR42 were of spectral type late-K V then it would be over-luminous by ∼2.5 magnitude. ASR42 is clearly a PMS object and we can only say that it is of spectral type later than mid-K V (over-luminous by ∼0.5 magnitude) and perhaps more likely, late-K V (over-luminous by ∼2-2.5 magnitudes).

ASR43 (SSV18b) is located intermediate to the l.c. V and l.c. III loci in Fig. 11. It lies on the reddening vector from the O-B V ZAMS star location in the JHK c-c diagram and in Paper I was classified as a PMS star on the basis of an NIR excess in the optical-NIR RIJK c-c diagram. In our JKL c-c diagram of Paper II ASR43 is located on the reddening vector extending from the cool end of the ZAMS/giant branch. With an m_K ∼10, ASR43 would be a F1 V star on the (unreddened) ZAMS at 318pc. However, it possesses Na I and Ca I absorption plus CO absorption inconsistent with the spectrum expected from a early-F V ZAMS star. Brγ appears slightly in emission in ASR43 suggestive of accretion activity near the stellar photosphere. If we assume ASR43 is an K2-3 V star (its l.c. V locus position by projecting its location parallel to the dotted lines in Fig. 11) and located at 318pc it would be over-luminous (after reddening [A_V ∼6] correction) by ∼2.5 magnitudes assuming an A_V ∼6 (dereddening to the T Tauri star locus in Fig. 4). As in ASR42, ASR43 has some H_2O absorption at 2μm but with its intermediate (l.c. V to l.c. III) absorption spectrum, it is unclear what this implies.

ASR44 is located on the l.c. I locus in Fig. 11 indicating the presence of a very low surface gravity supergiant-like atmosphere. In the JHK c-c diagram (Fig. 4) it lies close to the unreddened T Tauri star locus and was classified as a background mid-A V star with A_V=6 in Paper I from dereddening to the ZAMS. This is clearly an erroneous classification since ASR44 exhibits CO absorption and has no Brγ absorption. With an m_K ∼12.1, and assuming ASR44 is at 318pc, its implied ZAMS spectral type from its M_K (∼5 assuming A_V ∼0 by dereddening to the T Tauri star locus) would be late-K V. Such a star would have Na I and Ca I absorption at strengths equal to the v=2-0 CO bandhead. If ASR44 is of earlier spectral type then it would have to be under-luminous at 318pc. If ASR44 is a background l.c. I source as implied by its location in Fig. 11, it would be of spectral type K0 I at d>8kpc. The WGM92 galaxy model predictions (Table 4) rule out such a star being present in the NGC 1333S field. The low surface gravity nature of the absorption in ASR44 and the implication that it is a l.c. V star (i.e. not a l.c. I star) implies that ASR44 is a PMS star in the NGC 1333S cloud. With a classification of M0 V, ASR44 would be perhaps 0.5 magnitudes over-luminous. However, we have to reconcile its implied spectral type with its location in Fig. 11. Since it is reasonable to assume that the lower the surface gravity stellar atmosphere the young the star (i.e. as a low-mass PMS star evolved to the ZAMS its atmosphere becomes less extended and more like a l.c. V star), a low-mass PMS star with a l.c. I-like atmosphere must be very young and hence, more over-luminous (due to the larger radius) than a PMS star showing l.c. II–III–V atmospheric absorption. This assumes that the low surface gravity absorption comes from the stellar atmosphere and not the atmosphere of its accretion disk. Since ASR44 shows no thermal excess emission (from its location in the JKL c-c diagram in Paper II), it is likely that it is stellar, and not disk, atmospheric absorption we are observing. Thus, ASR44 should be more over-luminous than the above estimated 0.5 magnitudes for an implied spectral type of M1 V. For this to be true, ASR44 would have to be of later spectral type than M 1V. For an over-luminosity of 1, 2 and 3 magnitudes, ASR44 would be of spectral type ∼ M2 V, M3 V and M4 V, respectively.

ASR46 lies close to the position of ASR44 in Fig. 11 on the l.c. I locus. Its 2μm spectrum is very similar to that of ASR44 with the addition of a detection of weak Na I absorption. It has an m_K ∼0.5 magnitude fainter than ASR44 at 12.7 and has a small thermal IR excess from the JHK c-c diagram (Fig. 4). This implies that ASR46 is a PMS star located in the NGC 1333S molecular cloud. Its M_K at 318pc would be 5.2 (with A_V ∼0 dereddening to the T Tauri star locus) corresponding to a M0 V ZAMS star. With its implied low surface gravity atmosphere and the NIR thermal excess ASR46 is certainly a PMS star and not on the ZAMS. The low surface gravity spectral features imply that ASR46 should be over-luminous wrt its final classification on the ZAMS, hence it should be of later spectral type than that suggested by its M_K value. Our best estimate of the spectral type of ASR46 therefore is that it is later than M0 V. ASR46 would be over-luminous by 1, 2 and 3 magnitude, respectively, if it were an M2 V, M3 V or M4 V dwarf star.

ASR51 is located directly on the dwarf locus in Fig. 11 with an implied spectral classification of M3-4 V. In Paper I it was found to be close below (C_B) the ZAMS in the JHK c-c diagram and, under the assumption it is reddened background ZAMS star, was classified as a O-B V star with A_V=5. In Paper II its location in the JKL c-c diagram was consistent with it being a late-type dwarf rather than a reddened early-type star. Clearly ASR51 has a late-type dwarf spectrum and is not a distant O-B V star. Alternative interpretations of its location in the JHK c-c plot, shown here in Fig. 4, are that it could either possess a small thermal excess at K or photometric uncertainties have displaced it from the nearby cool end of the ZAMS. Since ASR51 shows no thermal excess in the JKL c-c diagram of Paper II we assume the latter explanation is the most likely. At 318pc, ASR51 would have a M_K of 3.9 approximately 3 magnitudes over-luminous for an M3 V classification and more typical of a late-G V ZAMS star. There is no indication in its 2μm spectrum of H_2O absorption at 2μm suggesting it is of earlier spectral type than M3 V i.e. at latest M1 V (see WGM99 Fig. 3 plot of H_2O index vs. spectral types). This result implies that the data on ASR51 is not consistent with it being a member of the NGC 1333S PMS stellar cluster. We consider that the data on ASR51 is consistent with it being an M1 V ZAMS star at a distance of 25pc since it is at this distance that the NIR photometry of ASR51 becomes consistent with the spectral type from its spectral features. Why its location in the JHK c-c diagram is inaccurate is perhaps understandable since in the coarsely sampled (1.2$''$/pixel) K band image of the region (Paper I Fig.1) it appears close to a non-stellar nebulous feature to the north-west. This association may have effected the derived photometry of ASR51 and resulted in an overly bright m_K. In the JHK c-c diagram, this would moved ASR51 away from the ZAMS. A brightness error of only ∼0.3 magnitudes would be necessary to place it in the appropriate early-M V regime.

In Paper I ASR56 was considered to be a reddened background star having a low (0 magnitude) derived A_V value. Under the assumption it is a K0 V star (its implied spectral types from dereddening), with absolute K magnitude, M_K, of 4.15, then from its m_K of 11.86, its distance was determined to be 350pc. In Fig. 11 ASR56 lies close to the l.c. III locus at positions typical of late-G to early K-III stars. Clearly this is inconsistent with its spectral type from

Paper I. Its 2μm spectrum shows a continuum declining to the red with weak Na I, Ca I and CO absorption. In the JHK c-c diagram (Fig. 4) ASR56 lies at an intersection between i) the ZAMS at early- to mid-K V, ii) the early-K III end of the giant branch and iii) and at the beginning of the unreddened T Tauri stars locus (from GM95). Thus, its location in Fig. 11 (late-G to early-K III) and one possible interpretation of its position in the JHK c-c diagram are consistent. If ASR56 is a background K1-2 III giant then it would have to be at a distance of 3.7kpc. The WGM89 galaxy model does predict that one K0-1 III giant might be present in the NGC 1333S field at a distance of 3–4kpc. Perhaps ASR56 is such a star. Since ASR56 is relatively unreddened it would have to be observed through a low extinction 'hole' through the NGC 1333S cloud if at such a distance. ASR56 is also one of only three sources to have relatively consistent fitted continuum (black-body) spectra in Section 3.6. Its derived T_{der} was 6000K with A_V=0 while the T_{eff} of a K1 III star is ∼4700K i.e. within the errors in the fitting. This also supports the interpretation that ASR56 is a background K1 III giant star. If we interpret ASR56 as a K0 V dwarf at 318pc then it would be in the NGC 1333S PMS cluster. Its giant-like atmospheric absorption (as implied from Fig. 11) would suggest it would be a PMS object in this interpretation. In light of these arguments, ASR56 is therefore either a relatively unreddened background early-K III giant (at ∼3-4kpc) or a PMS star in NGC 1333S over-luminous for its spectral type (due to its location in Fig. 11). For an over-luminosity of 1 magnitude, ASR56 would be a late-K V and for a larger over-luminosity of later spectral type still. However, its lack of strong Na I, Ca I and CO absorption suggests it is not later than K1 V. We tentatively suggest therefore, that the distant K1 III interpretation for ASR56 is more compelling.

ASR57 appears to be a peculiar object when its atomic and molecular indices are considered (see Table 5). However, its 2μm spectrum shows pure H_2 emission lines with little to no continuum emission over the K window. Its indices are clearly effected by the close proximity of H_2 lines to the continuum bands used to estimate the atomic and molecular indices (see Fig. 7). From the images of Hodapp & Ladd (1995) ASR57 appears to be a shock-excited nebula possibly originating in the bipolar outflow from IRAS4a.

ASR78 is located between the l.c. V and l.c. III loci in the low surface gravity atmosphere absorption regime near the locus joining the K5-M2 V and III sources. Its spectrum shows CO absorption and weak Ca I and Na I absorption. It was classified as an M0-6 III from dereddening considerations in Paper I implying it would be a distant (>5.7kpc) slightly reddened (A_V ∼4) background giant. However, the WGM92 galaxy model predicts a low probability of finding such an object in the NGC 1333S field. With m_K=11.3, ASR78 would have an (extinction corrected, dereddening to the ZAMS) M_K ∼3.4 at 318pc corresponding to a G5 V dwarf. ASR78 is also designated Lk Hα 355 and, by definition, shows (strong, as noted by Strom et al. 1986) optical Hα emission. No Brγ emission is seen in the 2μm spectrum however, implying that the H recombination emission from the source may be variable in nature. In Paper I ASR78 was classified as an PMS object on the basis of its association with optical Hα emission. We conclude here therefore that ASR78 is likely a PMS star based on the previous detection of Hα emission, its location in Fig. 11 i.e. in the intermediate surface gravity regime, and the WGM92 model predictions. Its location in Fig. 11 suggests that ASR78 should be considerably over-luminous wrt to its final ZAMS spectral type (i.e. since it exhibits giant-like atmospheric features). ASR78 shows no significant H_2O absorption and its NIR JHK colours (Fig. 4, dereddening to the dwarf locus) suggests it to be of spectral type between early-K V (A_V ∼7) and M2 V (A_V ∼4). If we deredden to the T Tauri star locus shown in Fig. 4 we obtain a spectral classification of mid-K V implying an M_K ∼4.3, and about 1 magnitude over-luminous. At a spectral type of M0 V (the latest spectral type without significant H_2O absorption) ASR78 would be ∼2 magnitude over-luminous. This is more consistent (than a mid-K V classification) with its location in Fig. 11 and is still reconcilable with its JHK photometry/colours.

ASR86 is located mid-way between the l.c. V and l.c. III loci in Fig. 11 implying the presence of low surface gravity (giant-like) atmospheric absorption. In Paper I is was classified as a reddened background A6-9 V star based solely on dereddening (A_V=13) onto the ZAMS. Reddening to the cool end of the dwarf locus in the JHK c-c diagram gives a spectral type of mid-M V with A_V ∼8. The 2μm spectrum of ASR86 shows reasonably strong CO, absorption and a good detection of both Na I and Ca I absorption. Clearly, ASR86 is not a background A V star. At m_K=12, ASR86 would be an late-G V ZAMS star (with M_K=3.7, extinction corrected) at 318pc. Since it possesses intermediate-surface gravity absorption, ASR86 is likely a PMS object in NGC 1333S. Tracing the location of ASR86 back to the l.c. V locus in Fig. 11 (parallel to the dotted lines) suggests a mid-K V to early-M V classification with, however, intermediate surface gravity atmospheric absorption. No significant H_2O absorption at 2μm suggests a spectral type earlier than M0 V. We conclude that the most likely interpretation of the observations of ASR86 is that it is an early-M V PMS star over-luminous by ∼1.5 magnitudes. ASR86 may therefore possess a small thermal excess at 2μm to reconcile its location in the JHK c-c diagram with an early-M V spectral classification.

ASR105 lies close to the l.c. III locus in Fig. 11 and classified a PMS star in Paper I on the basis of its JHK colours (see Fig. 4) i.e. it possesses a small thermal excess at 2μm lying below the reddening vector from the high-mass end of the ZAMS yet within the (reddened) extreme of the T Tauri star locus. With an m_K of 12.4, dereddening (to the T Tauri locus giving $A_V \sim 3$) results in an M_K (at 318pc) of 4.6 and an implied spectral classification of late-K V (ZAMS). ASR105 possesses intrinsic H_2 emission (the v=1-0 S(1) line at 2.122μm, intrinsic since other stars nearby, e.g. ASR7, ASR8, do not show such emission) as well as CO absorption and possible weak detections of Na I and Ca I absorption. Its Na I strength in Table 5 may be effected by the weak emission 'bump' in the short-wavelength Na I continuum band. Compensating for this artifact results in ASR105 moving further towards the l.c. I locus in Fig. 11. In the JKL c-c diagram of Paper II, ASR105 shows a 3μm thermal excess implying the presence of heated circumstellar dust. ASR105 is therefore a relatively low extinction PMS T Tauri star in NGC 1333S. Tracing its location in Fig. 11 back to the l.c. V locus (parallel to the dotted lines) implies a spectral classification of ~K3 V. However, this results in ASR105 being under-luminous (by ~0.5 magnitudes) for its inferred spectral type. It would be necessary to place ASR105 at 350pc (outwith the NGC 1333S SFR assuming d=318pc) to obtain agreement between the spectroscopic and photometric spectral classifications and at this distance ASR105 would be an early-K V star with no luminosity excess. Assuming ASR105 is at 318pc implies a spectral type of late-K V which, in order to possess an over-luminosity wrt its ZAMS spectral classification, is an upper limit (i.e. ASR105 has to be later than this spectral type). Since there is little to no evidence for H_2O absorption at 2μm in the spectrum of ASR105, its spectral type must be at latest early-M V. If we assume a spectral type of M0-1 V then ASR105 would be a PMS over-luminous by ~1-1.5 magnitudes.

ASR106 (SSV16) shows a relatively featureless rising red continuum spectrum at 2μm. Above, it was modeled by a 3000K black-body with $A_V \sim 35$ (Table 3) and in the Paper I JHK c-c diagram shows highly reddened colours interpreted there as being a reddened O-B V star. In Paper II it was found to exhibit a large 3μm thermal excess indicative of a heavily obscured 'Class I' PMS star. In Fig. 11 ASR106 lies close to zero in both atomic and molecular indices and hence the atomic and molecular indices are of little use in determining its underlying spectral classification. If we deredden ASR106 to the T Tauri locus in Fig. 4 we obtain an extinction of A_V=18 and hence (for its m_K of 10.4), an extinction corrected M_K of ~1.1 equivalent to an early-A V ZAMS star. Thus, all we can say regarding ASR106 is that it is a deeply embedded low- to intermediate-mass PMS object in NGC 1333S. There is a suggestion, however, of H_2O absorption at 2μm (see Fig. 7). Since such absorption should only occur in ZAMS stars of spectral type M0 V or later, ASR106 would have to over-luminous by ~4 magnitudes to give the above M_K value. This would be consistent with its obvious young state. However, we should also see Na I, Ca I and CO absorption at that spectral type. One possibility is that thermal emission is veiling such emission while it is not as effective at 2μm.

ASR107 also shows a relatively featureless rising red continuum. Brγ emission is weakly present and there is an indication of very weak CO and Ca I absorption features. In both Paper I and II, ASR107 was classified as a PMS object due to the NIR excess emission visible in JHK and JKL c-c diagrams. It was also found to possess diffuse nebulous emission in the JHK images. Its m_K of 10.5 suggests a spectral type of mid-F V ZAMS from its extinction corrected (A_V=4 at d=318pc) M_K of 2.6 (dereddening to the T Tauri star locus in Fig. 4). From Fig. 11 its small atomic and molecular indices preclude an accurate determination of spectral classification. All we can say is that ASR107 is certainly an embedded PMS object in the NGC 1333S cloud. No obvious H_2O absorption is seen at 2μm suggesting it may be of earlier spectral type than M0 V. At M0 V in the NGC 1333S cluster at 318pc, ASR107 would be over-luminous by 2.5 magnitudes. This is, however, inconsistent with its location in Fig. 11 which implies perhaps a spectral type more like K2 V. At K2 V, ASR107 would be over-luminous by 1.5 magnitudes. We adopt this interpretation as the most consistent with all the data available.

ASR111 shows CO absorption but little to no Na I and Ca I absorption in its 2μm spectrum and is hence located well below the dwarf and giant loci in Fig. 11 lying even below the l.c. I supergiant locus. It also lies below the reddened ZAMS in the JHK c-c diagram (Fig. 4) and was classified as a PMS object in Paper I. It m_K of 10.8 (at 318pc) implies an $M_K \sim 3.3$ indicative of an mid-G V ZAMS star. This classification is clearly inconsistent with that from Fig. 11. To possess absorption characteristics indicative of a very low surface gravity atmosphere would suggest that ASR111 is young and hence possesses a significant over-luminosity wrt to its final ZAMS classification. Since there is no obvious H_2O absorption in its 2μm spectrum (see Fig. 7) the latest spectral type ASR111 could be is early-M V. At mid-K V ASR111 would be over-luminous by ~1 magnitude. At M0 V, this over-luminosity becomes ~3 magnitudes.

ASR112 (SSV5, HH17) is another source showing little 2μm structure. In our high signal:noise spectrum weak CO bands and Ca I absorption are possible present in absorption (but not significant in terms of a molecular and atomic indices in Fig. 11) and there is no indication of Na I absorption (see Fig. 7). ASR112 has m_K=10.3 and appears heavily reddened in the JHK c-c diagram. In the JKL c-c diagram of Paper II ASR112 has a large 3μm excess implying the presence of heated dust and a certain PMS evolutionary state. Dereddening to the T Tauri star locus in Fig. 4 implies an $A_V \sim 15$. With a extinction corrected M_K of 1.3 the implied spectral type of ASR112 from its photometry is mid-A V and hence, this is the earliest spectral type ASR112 can be to have an intrinsic over-luminosity (for a PMS object). Weak CO and Ca I imply perhaps significantly later spectral type although these feature may originate in the circumstellar material (disk) around the source. For a 1 magnitude over-luminosity, ASR112 would be required to be of spectral classification mid-F V. For mid-K V, this becomes ∼3 magnitudes.

ASR113 lies close to (but slightly on the intermediate surface gravity side of) the l.c. V locus in Fig. 11 and has an implied spectral classification of M3-4 V. It is located below the ZAMS in the JHK c-c diagram (Fig. 4) close to the locus of unreddened T Tauri stars and was hence classified as a PMS star in Paper I. If ASR113 is an unreddened T Tauri star in NGC 1333S cloud then it would have an M_K of 2.8 equivalent to that of a F8 V ZAMS star. If ASR113 is a early- to mid-M V star on the ZAMS then it would be at a distance of d<50pc. However, this would not be consistent with the small thermal excess seem in its JHK colours. ASR113 is physically located within the nebulous complex of optical emission called HH 12 in NGC 1333S (see Fig. 3 in Paper I). It has a close companion, ASR115, some $\sim 6''$ away which is remarkably similar photometrically (see Paper I Table 3) and spectroscopically (see Fig. 7) although due to local continuum irregularities near Na I and somewhat deeper CO absorption, ASR115 has a considerably larger atomic and molecular indices. In our combined optical-NIR RIJK c-c diagram (see Fig. 15 in Paper I), ASR113 appears as a reddened late-M V and hence, inconsistent with its JHK c-c diagram location and spectral type from the atomic and molecular indices plot (Fig. 11). The close physical association with HH 12, its NIR photometric similarity to an unreddened T Tauri star, and its inconsistent optical-NIR classification all suggests that ASR113 is a PMS object. If ASR113 is an M3-4 V star it would be ∼4 magnitudes over-luminous. To obtain a 2 magnitude over-luminosity, ASR113 would have to be of spectral classification late-K V. There is no indication of H_2O absorption at 2μm and hence ASR113 should be at latest of spectral type M0 V. Thus, it seems that the most consistent interpretation of available data on ASR113 is that it is late-K V with a 2 magnitude over-luminosity.

ASR114 (SSV12) is a very red source with a steep rising red continuum over its 2μm spectrum. Its JHK colours show the presence of thermal excess emission. ASR114 shows H_2 emission but no other features in its 2μm. At an m_K of 10.6 its implied (extinction corrected [A_V=7] to the T Tauri star locus in Fig. 4) M_K is 2.4 corresponding to a ZAMS star of spectral type mid-F V. Since no atomic or molecular absorption features are present in its 2μm spectrum we cannot confirm a spectral classification spectroscopically. However, we can confirm its PMS origin from the non-photospheric nature of its 2μm spectrum, the presence of H_2 emission and its JHK thermal excess.

ASR115 is located in the intermediate surface gravity zone in Fig. 11 closer to the l.c. III locus than that of l.c. V sources. Its m_K of 10.7 and JHK colours suggested it was a background mid- to late-B V star in Paper I, a conclusions clearly inaccurate when its 2μm spectrum is considered. With the above m_K and at 318pc, ASR115 would have an (extinction corrected, A_V=3) M_K of 2.9 corresponding to a late-F V star. This also is inconsistent with the NIR spectral features present. There is a suggestion of H_2O absorption at 2μm (see Fig. 7) implying ASR115 has a spectral type later than M0 V. If we assume a spectral type of early-M V (with a corresponding $M_K \sim 5.8$) then ASR115 would be over-luminous by ∼3 magnitudes and would be a PMS object. If we trace the location of ASR115 in Fig. 11 back to the l.c. V locus (parallel to the dotted lines) we obtain a spectral classification of ∼early-M V. We therefore conclude that the most likely interpretation of the data on ASR115 is that it is of spectral classification early-M V and is over-luminous wrt the the ZAMS by ∼3 magnitudes a fact supported by its intermediate surface gravity absorption features.

ASR118 (SSV15) has a relatively flat spectrum through the 2μm window. It shows CO absorption and both weak Ca I absorption and H_2 emission. In Fig. 11 it is located in the l.c. III and l.c. I regime with a small atomic absorption index and a significant molecular index. In the JHK c-c diagram (Fig. 4) ASR118 shows a small thermal excess and lies in the reddened T Tauri star region. In the JKL c-c diagram of Paper II it shows a larger thermal excess indicating its PMS origin. With an m_K of 9.9 its extinction corrected (by A_V=4 to the T Tauri star locus) M_K (at 318pc) is 2.0, corresponding to a early-F V star. Likely ASR118 is of later spectral type than this since it is certain a PMS object, has low surface gravity 2μm absorption and should be over-luminous for its spectral type. In addition, a late-F V ZAMS star would not possess significant CO absorption. At early-K V, ASR118 would be over-luminous by ∼2 magnitudes. This is our best estimate of the spectral classification of ASR118.

ASR120 (SSV11) is located close to the higher temperature end of the dwarf locus in Fig 11. This corresponds to a l.c. V star of spectral type early-K V. Its spectrum shows Brγ emission plus weak CO, Ca I and Na I absorption indicating the presence of a cool photosphere as well as a source of ionization. ASR120 is also designated SSV11 and was classified in Paper I as being associated with optical and NIR nebulosity. Its location in the JHK c-c diagram of Paper I (Fig. 4 here) implies a moderately reddened ($A_V \sim 12$) early-type star inconsistent with the presence of the atomic and molecular absorption features observed. In the thermal NIR JKL c-c diagram its location was approximately consistent with that found in the JHK c-c plot although it may possess a modest NIR thermal excess. Since its 2μm spectrum implies a considerably later spectral type than the O-B V value obtained from dereddening i.e. early-K V, a small thermal excess at K could also be present in the JHK c-c diagram. Assuming ASR120 is a reddened T Tauri star (cf. the T Tauri star locus in Fig. 4) it would have $A_V \sim 6$. The implied M_K for ASR120, assuming d=318pc, is 0.9 (extinction corrected) implying that on the ZAMS it would be an early-A V star. Assuming ASR120 is a early-K V would mean it is ~3 magnitude over-luminous. ASR120 should therefore be classified as a PMS object on the basis of the presence of H recombination emission in its spectrum together with atomic and molecular absorption, the presence of a small thermal excess longwards of 2μm and its implied over-luminous nature.

ASR121 has a relatively flat 2μm spectrum with the addition of CO absorption bands and Ca I absorption plus likely Na I absorption (the latter is partly masked by a bad pixel 'glitch' on the detector). In Fig. 11 it is located in the intermediate surface gravity region between the l.c. V and l.c. III loci. The effect of the array glitch at Na I on the atomic index is to increase its value (increasing the local continuum on the blueward side of the line) and so, the atomic index should be perhaps 50% of the displayed value moving ASR121 more into the l.c. III regime of the plot. In the JHK c-c diagram from Paper I (Fig. 4 here) ASR121 is slightly below the reddening vector from early-type ZAMS stars. Dereddening to the ZAMS implies an $A_V \sim 7$ and it was interpreted as a reddened O-B V star in Paper I. Clearly this is erroneous and ASR121 contains a cool, low surface gravity atmosphere. In the JKL c-c diagram of Paper II ASR121 appears to lie close to the unreddened giant branch and shows no thermal excess emission. With an m_K of 10.4, ASR121 has a dereddened (dereddened to the cool end of the ZAMS not the hot end as in Paper I) M_K of ~2.7 implying it would be a late-F V star if located on the ZAMS and at 318pc. If ASR121 was a background G III giant (as implied by its location in Fig. 11) it would be at ~2kpc. As we have seen from the WGM92 model predictions, the probability of finding such a giant towards NGC 1333S is very low. We conclude therefore that ASR121 is a PMS object in the NGC 1333S cloud. Tracing its location in Fig. 11 back to the l.c. V locus suggests a spectral type of perhaps mid-K V. If this is correct then ASR121 would be over-luminous wrt to its final ZAMS location by 1.5 magnitude. This conclusion is supported by the necessity for an over-luminosity (due to its low surface gravity absorption features).

ASR122 (SSV10 and LkHα352a) is located on the l.c. V locus in Fig. 11 at the K0 V position. It possesses Brγ emission which implies the presence of a source of ionizing radiation in addition to a cooler region producing atomic and molecular absorption. In the JHK c-c diagram ASR122 appears to be a early-K V star reddened by $A_V \sim 9$ magnitudes at 60pc but was classified as a PMS star on the basis of associated H recombination emission and a significant reddening combined with a small distance. In our JKL c-c diagram from Paper II, it was found to possess a significant thermal excess implying the presence of a heated circumstellar envelope, likely an inclined disk since the source is optically visible. From its $m_K \sim 9$ and d=318pc we obtain a dereddened (to the T Tauri star locus) $M_K \sim 1.5$ equivalent to a mid-A V ZAMS star. For a early-K V star this implies an over-luminosity of ~2.5 magnitudes. We conclude that ASR122 is therefore a young, over-luminous T Tauri PMS star of spectral type early-K V. At the hotter end of the l.c. V and l.c. III loci the absorption characteristics of dwarfs and giants appear similar in a atomic vs. molecular indices plot, this could easily mask low surface gravity absorption likely present for such an over-luminosity.

ASR123 (SSV20 and Lk Hα 271) lies close above (C_A) the reddened ZAMS in our JHK plot (Fig. 4). This is the only source, with any degree of consistency between the T_{der} and T_{eff} values in Section 3.6, that was classified as a possible PMS star. In this case the classification was based on associated Hα emission. Its 2μm spectrum confirms this since it shows Brγ in emission. ASR123 also possesses weak Na I and Ca I absorption and possibly (very) weak CO absorption. Its implied M0-6 III (dereddening based) spectral classification from Paper I is clearly in error. In Fig. 11 it lies slightly above the l.c. V locus (since it has good detections of Na I and Ca I absorption but very weak CO absorption) close to the K0 V star position. Placing ASR123 at 318pc and dereddening to the T Tauri star locus (m_K=9.4, $A_V \sim 9$), would require it to have an $M_K \sim 1$ equivalent to a early-A V ZAMS star. This implies that ASR123 is over-luminous for its (later, early-K V) spectroscopic spectral classification. It appears from all considerations (including association with H recombination emission) that ASR123 is a PMS stars associated with NGC 1333S. If we assume ASR123 is a K0 V PMS stars at 318pc then it is over-luminous by ~3 magnitudes.

ASR125 is located between the l.c. V and l.c. III loci in Fig. 11. Its 2μm spectrum shows Na I, Ca I and CO absorption features and a declining blue continuum. In the JHK c-c diagram of Paper I it was interpreted as a PMS object on the basis of a derived distance modulus <7.7 (350pc) with an A_V >5 magnitudes even though its NIR colours were consistent with it being a reddened ($A_V \sim 5$) early-G V ZAMS star. If ASR125 is a PMS object it could be a less reddened ($A_V \sim 3$) T Tauri star (see Fig. 4). From its m_K of ~10, its extinction corrected (dereddening to the T Tauri star locus in Fig. 4, $A_V \sim 4$) M_K of ~ 2 (at 318pc) implies a spectral type of early-F V inconsistent with dereddening onto the ZAMS in the JHK c-c diagram. Tracing its location in Fig. 11 back to the l.c. V locus (parallel to the dotted lines) implies a spectral classification of K2-3 V. With its intermediate surface gravity absorption features, ASR125 is certainly not an early-F V ZAMS star. We rule out the possibility of it being a distant (1.3kpc) K3 III giant (the closest l.c. III source to its location in Fig. 11) from the WGM92 model predictions. Our best estimate for the spectral type of ASR125 is that it is an early- to mid-K V PMS star based on its dwarf nature with intermediate surface gravity absorption. This would make it over-luminous by ~ 2 magnitudes.

ASR128 (SSV21, Lk Hα 351) lies in the intermediate surface gravity region of Fig. 11 between the l.c. V and l.c. III loci. In the JHK c-c diagram (Fig. 4) ASR128 lies along a reddening vector from both the cool end of the ZAMS and the T Tauri star locus. In Paper I it was consistent with being a mid- to late-G V reddened by $A_V \sim 4$ although it was classified as a PMS star on the basis of associated Hα emission. No corresponding Brγ emission is seen at 2μm however suggesting that H recombination emission from the source may be variable. Tracing its location in Fig. 11 back to the l.c. V locus (parallel to the dotted lines) results in a spectral classification of mid-K to early-M V. From its m_K of 9.6, its dereddened (A_V=4) M_K is ~ 1.7 suggesting a ZAMS spectral classification of mid-A V. This implies ASR128 is over-luminous for its dereddened spectral type (assuming a late-K V) by ~ 3 magnitudes. ASR128 is clearly a PMS object since it has Hα emission and a giant-like 2μm absorption spectrum. The predictions of the WGM92 galaxy model rule out the presence of a mid-K III star (the closest to the location of ASR128 in Fig. 11) with this m_K along this line-of-sight through the galaxy. We therefore adopt the classification of late-K V with a 3 magnitude over-luminosity for ASR128.

ASR130 (BD+30547, SSV19) is located in the region intermediate to l.c. III and l.c. I stars (at the hotter end of the spectral range) in Fig. 11. It shows Brγ absorption, no Na I absorption but very weak Ca I and CO absorption and possibly very weak H_2O absorption in its high signal:noise 2μm spectrum. It was implied to be reddened background star having a low (2 magnitudes) derived A_V value. Assuming this source is an A6 V star (its implied spectral types from dereddening) with an M_K of 0.0 then with an m_K of 7.7 it would be at a distance of $\sim$150pc. This implied distance is somewhat smaller than our working estimate for NGC 1333S i.e. 318pc suggesting that ASR130 has a earlier classification that A6 V. A classification of B7 V would be required to located the source in the NGC 1333S molecular cloud. The presence of weak Ca I and CO absorption is clearly not consistent with an early-A V classification and implies that ASR130 may not be a single star but have a cool, faint companion. Significant CO, Ca I and H_2O absorption occurs in mid-M V stars and later and, if the feature observed in the spectrum of ASR130 can be confirmed, would imply its companion is a low-mass object. Alternatively, the atomic and molecular absorption could originate in circumstellar material around the star, perhaps the remnants of an envelope or disk, although no significant NIR excess is observed. ASR130 seems to be a ZAMS late-B V star but has several peculiar characteristics warranting further observation.

Table 1
Details of sources observed in NGC 1333S

ASR[a]	Other ID[b]	m_K[c] (mags)	CwR[d]	A_V[e] (mags)	Implied[f] Sp. Type	Possible PMS[g] star ?
1	SSV13	8.25	N			Y
2		11.86	Y	2	K0-3V	
7	SSV14	9.66	Y	20	M3-6III	
8		12.21	Y	7	O3-9V	Y [j]
24		12.86	Y	7	B6-9V	Y [m]
36	SSS107	11.39	Y	2	K3-6V	Y [l]
37		12.24	Y	7	B6-9V	Y [k]
40		11.17	C_A[h]	15	M0-6III	
42	SSV18a	11.65	Y	6	G6-9V	Y [k]
43	SSV18b	9.96	Y	17	O6-9V	Y [m]
44		12.15	Y	6	A6-9V	
46		12.67	N			Y
51		11.44	C_B[i]	5	O-B	
56		11.86	Y	0	K0-3V	
57		12.84				
78	Lk Hα 355	13.50	C_A[h]	4	M0-6III	Y [l]
86		11.98	Y	13	A6-9V	
105		12.39	N			Y
106	SSV16	10.39	C_B[i]	32	O-B	
107		10.52	N			Y
111	SSV17	10.76	N			Y
112	SSV5,HH17	10.31	Y	8	K0-3V	Y [k]
113		10.43	N			Y
114	SSV12	10.61	N			Y
115		10.65	Y	8	B6-9V	
118	SSV15	9.90	N			Y
120	SSV11	9.56	C_B[i]	16	O-B	Y [m]
121		10.38	C_B[i]	7	O-B	
122	SSV10, Lk Hα 352a	9.09	Y	9	K0-3V	Y [k*l*]
123	SSV20, Lk Hα 271	9.41	C_A[h]	7	M0-6III	Y [l]
125		9.97	Y	8	G0-3V	Y [k]
128	SSV21, Lk Hα 351	10.19	Y	4	G6-9V	Y [l]
130	SSV19,BD+30547	7.66	Y	2	A6-9V	

[a] ASR catalog number given in Paper I

[b] Name from work prior to Paper

[c] Apparent K magnitude of source

[d] Position in J-H vs. H-K diagram is consistent with a reddened ZAMS star

[e] Derived visual extinction (dereddening to ZAMS) if source CwR=Y or C_A/C_B

[f] Implied spectral type from dereddening in Paper I

[g] Evolutionary status determined in Paper I

[h] Lies Close-Above upper reddening vector in the J-H vs. H-K diagram in Paper I

[i] Lies Close-Below lower reddening vector in the J-H vs. H-K diagram in Paper I

[j] Implied from m-M>13.9==6kpc in Paper I

[k] Implied from m-M<7.7 + implied an A_V >5 in Paper I

[l] Implied from associated Hα emission in Paper I

[m] Implied from optical R-I vs vs. J-K diagram in Paper I

TABLE 2

FLUXES OF SOURCES OBSERVED IN NGC 1333S

ASR[a]	Flux 2.05μm (W m^{-2} μm^{-1})	Flux 2.25μm (W m^{-2} μm^{-1})	Flux 2.43μm (W m^{-2} μm^{-1})
1	1.17×10^{-13}	1.34×10^{-13}	1.88×10^{-13}
2	7.37×10^{-15}	6.47×10^{-15}	4.41×10^{-15}
7	2.81×10^{-14}	3.17×10^{-14}	3.58×10^{-14}
8	4.41×10^{-15}	4.68×10^{-15}	2.80×10^{-15}
24	2.62×10^{-15}	2.81×10^{-15}	1.67×10^{-15}
36	8.64×10^{-15}	7.75×10^{-15}	6.82×10^{-15}
37	3.74×10^{-15}	4.32×10^{-15}	2.76×10^{-15}
40	1.26×10^{-14}	1.61×10^{-14}	1.50×10^{-14}
42	8.10×10^{-15}	8.77×10^{-15}	6.10×10^{-15}
43	2.81×10^{-14}	2.85×10^{-14}	2.19×10^{-14}
44	4.28×10^{-15}	4.64×10^{-15}	2.70×10^{-15}
46	4.34×10^{-15}	4.52×10^{-15}	3.05×10^{-15}
51	1.10×10^{-14}	1.04×10^{-14}	7.82×10^{-15}
56	7.44×10^{-15}	5.90×10^{-15}	4.04×10^{-15}
57[b]	nc[c]	1.30×10^{-15}	nc[c]
78	1.16×10^{-14}	1.20×10^{-14}	6.96×10^{-15}
86	4.31×10^{-15}	4.55×10^{-15}	3.31×10^{-15}
105	3.31×10^{-15}	4.07×10^{-15}	2.58×10^{-15}
106	2.99×10^{-14}	4.29×10^{-14}	5.10×10^{-14}
107	1.13×10^{-14}	1.26×10^{-14}	1.37×10^{-14}
111	1.14×10^{-14}	1.37×10^{-14}	9.84×10^{-15}
112	2.47×10^{-14}	2.76×10^{-14}	2.89×10^{-14}
113	1.17×10^{-14}	1.24×10^{-14}	9.52×10^{-15}
114	8.92×10^{-15}	1.50×10^{-14}	2.21×10^{-14}
115	1.75×10^{-14}	1.83×10^{-14}	1.29×10^{-14}
118	4.38×10^{-14}	5.00×10^{-14}	4.34×10^{-14}
120	6.16×10^{-14}	5.59×10^{-14}	4.88×10^{-14}
121	2.23×10^{-14}	2.19×10^{-14}	1.49×10^{-14}
122	6.26×10^{-14}	5.55×10^{-14}	4.72×10^{-14}
123	2.17×10^{-14}	1.92×10^{-14}	1.51×10^{-14}
125	4.53×10^{-14}	4.24×10^{-14}	3.58×10^{-14}
128	6.34×10^{-14}	5.94×10^{-14}	3.99×10^{-14}
130	3.95×10^{-13}	3.08×10^{-13}	2.28×10^{-13}

[a] ASR catalog number given in Paper I

[b] Emission line source

[c] nc means no continuum emission detected

Table 3
Spectral features in sources observed

ASR[a]	Cont. Slope	H line ($B\gamma$)	H_2 lines emission	Na I/Ca I (2.21/2.26μm)	CO 2.294μm	T_{der}[b]/A_V[c] (K/mags)	T_{eff}[d] (K)
1	r/sh[e]	e[j]	e	e/n[l]	e	1175K	
2	b/st[h]	n	n	a[k]/a	a	2500K/2	4800−5240K
7	r/sh	n	n	a/a	a	2500K/20	3250−3630K
8	r/sh	n	we?[n]	wa[g]/wa	a	1500K/7	>33000K
24	r/sh	n	n	n/n	a	1500K/7	10000−14100K
36	b/sh[g]	n	n	a/a	a	2000K/2	4190−4780K
37	r/sh	n	n	n/n	a	1500K/7	10000−14100K
40	r/sh	n	we[m]	n/wa	wa	1500K/15	3420−3820K
42	r/sh	n	n	wa/wa	a	1500K/6	5300−5620K
43	f[i]	we	we	wa/a	a	3000K/13	>33000K
44	f	n	n	n/wa	a	1500K/6	7200−8000K
46	r/sh	n	n	wa/wa	a	1200K	
51	b/sh	n	n	a/a	a	2000K/5	>20000K
56	b/st	n	n	wa/wa	n	6000K/0	4800−5240K
57	n	n	e	n/n	n		
78	f	n	n	wa/wa	a	1500K/4	3250−3820K
86	r/sh	n	n	wa/wa	a	1500K/13	7200−8000K
105	r/sh	n	e	wa?[p]/wa?	a	1500K/17	
106	r/st[f]	n	n	n/n	n	3000K/35	>20000K
107	f	we	n	n/wa?	wa?	3000K/22	
111	r/sh	we	n	n/n	a	1500K/15	
112	r/sh	n	n	n/n	n	1400K/8	4800−5240K
113	f	n	n	wa/a	a	1500K/3	
114	r/st	n	e	n/n	n	600K	
115	f	n	n	a/a	a	2500K/8	10000−14100K
118	r/sh	n	we?	wa?/wa	wa	1100K	
120	b/sh	e	n	wa/wa	wa?	5000K/16	>20000K
121[e]	f	n	n	?[f]/a	a	2000K/7	>20000K
122	b/sh	e	n	wa/wa	wa?	2500K/9	5100K
123	b/sh	e	n	a/wa	n	3000K/7	3200−3800K
125	b/sh	n	n	wa/wa	a	2500K/8	4800−5240K
128	b/sh	n	n	a/a	a	2500K/6	5300−5620K
130	b/st	a	n	n/n	n	8000K/2	7200−8000K

[a] ASR catalog number given in Paper I

[b] Derived T_{eff} from the best-fit Planck function

[c] Visual extinction from dereddening to the ZAMS in Paper I

[d] Derived from dereddening onto ZAMS in J-H vs. H-K

[e] Feature masked by bad telluric correction

[f] Feature at 2.2μm is an artifact, partly masks Na I abs

Note.—r/sh = Shallow continuum rising to red. r/st = Steep continuum rising to red. b/sh = Shallow continuum rising to blue. b/st = Steep continuum rising to blue. f = Flat spectrum over observed wavelength range. e = Feature clearly in emission. a = Feature clearly in absorption. n = Feature not present. we = Feature clearly weakly in emission. we? = Feature possibly weakly in emission. wa = Feature clearly weakly in absorption. wa? = Feature possibly weakly in absorption.

TABLE 4
WGM92 GALAXY MODEL PREDICTIONS

Spectral	m_K [a] (mags)	Predicted[b] Sources No.	Distance[c] Range (pc)
F0-5 V	12	1 (1)	760−1200
F0-5V	13	1 (0)	1200−1900
F8 V	12	1 (1)	550−880
F8 V	13	1 (0)	880−1390
G0-2 V	13	1 (0)	730−1150
G5 V	12	1 (1)	390-620
G5 V	13	2 (0)	620−980
G8-K3 V	12	1 (1)	310−490
K4-5 V	13	1 (0)	440−700
M0-1 V	13	1 (0)	250−390
K0-1 III	11	1 (1)	3000−4700
K0-1 III	12	1 (1)	4700−7400

[a]Apparent K magnitude of the source

[b]Number of sources of this spectral type and magnitude likely to be present in the unreddened NGC 1333S field. The numbers in parentheses are the predicted source number after reddening by the NGC 1333S average A_V of 7 magnitudes

[c]Likely distance of the predicted sources

Table 5
Atomic and Molecular Indices

ASR[a]	Modified KH86 Atomic Index (Å)[b]	KH86 Molecular Index (Å)[b]
1[c]	-5.0	-20.6
2	8.7	7.3
7	2.2	5.4
8	2.9	9.3
24	0.5	9.9
36	9.9	6.9
37	0.4	9.5
40	3.3	4.1
42	3.1	7.7
43[d]	3.4	5.2
44	1.3	10.0
46[d]	1.0	8.4
51	7.2	7.4
56	2.6	4.8
57[f]	153.4	15.2
78	4.4	8.6
86	5.1	7.5
105[d]	3.5	6.7
106	1.4	0.7
107[c]	2.4	2.6
111[d]	-1.3	6.3
112	0.6	0.8
113	7.4	8.4
114	-2.0	-2.2
115	15.8	10.2
118	0.5	5.0
120[c]	3.6	1.7
121	4.7	8.6
122[c]	2.8	2.3
123[c]	3.6	1.8
125	3.7	5.6
128	4.9	8.8
130[e]	0.8	3.0

[a] ASR catalog number given in Paper I

[b] +ve = absorption, -ve = emission

[d] Brγ emission

[e] possibly weak Brγ emission

[f] Brγ absorption

[g] no continuum, just H_2 emission

TABLE 6
DERIVED EVOLUTIONARY STATE PARAMETERS

ASR[a]	PMS Star[b] (Paper I)	PMS Star[c] (Paper II)	PMS Star[d] (Here)	M_K[e] (Mags)	Proposed[f] Spectral Type	Over-Luminous[g] wrt ZAMS
1	Y	Y	Y	0.7	–	–
2	N	N	N	7.5	M3-4 V	–
7	N	N	Y	0.7	late-G V	3.5
8	Y		Y	4.7	early-K V	0.6
24	Y		Y	5.4	M4 V	3
36	Y	N	Y	4.4	M0 V	1
37	Y	N	Y	4.7	M4 V	3.5
40	?	Y	Y	2.2	K0 V	2
42	Y	N	Y	3.5	late-K V	2
43	Y	N	Y	1.9	K2-3 V	2.5
44	N	N	Y	5.0	M3 V	2
46	Y		Y	5.2	M3 V	2
51	?	N	N	3.9	M1 V	–
56	N		N	-1.5	early-K III	–
57	N		Pure H_2 Emission Nebulosity			
78	Y		Y	3.4	M0 V	2
86	N		Y	3.7	early-M V	1.5
105	Y	Y	Y	4.6	M0-1 V	1-1.5
106	?	Y	Y	1.1	M0 V	4
107	Y	Y	Y	2.6	K2 V	1.5
111	Y		Y	3.3	late-K V	2
112	Y	Y	Y	1.3	early-K V	2
113	Y		Y	2.8	late-K V	2
114	Y		Y	2.4	?	
115	N		Y	2.9	early-M V	3
118	Y	Y	Y	2.0	early-K V	2
120	Y	Y	Y	0.9	early-K V	3
121	?	N	Y	2.7	mid-K V	1.5
122	Y	Y	Y	1.5	early-K V	2.5
123	Y	Y	Y	1.0	early-K V	3
125	Y		Y	2.0	early- to mid-K V	2
128	Y		Y	1.7	late-K V	3
130	N	N	N	0.0	late-B V[h]	–

[a] ASR catalog number given in Paper I

[b] Implied to be a PMS object in Paper I

[c] Implied to be a PMS object in Paper II

[d] Implied to be a PMS object in this paper

[e] Absolute K magnitude (assuming d=318pc)

[f] Spectral type inferred from 2μm spectroscopy

[g] Magnitudes the source is over-luminous wrt ZAMS

[h] Peculiar, indication of presence of cool component

Table 7

H-R diagram data

ASR[a]	M_K [b] (mags)	Spectral Type[c]	T_{eff} [d] (K)	V-K[e] (mags)	M_V [f] (mags)	BC_V [f] (mags)	M_{bol} [f]	Log $L/L_\odot$ [g]	Log T_{eff}
2	7.5	M3-4 V	3420	4.9	12.4	-2.3	10.1	-2.15	3.53
7	0.7	late-G V	5520	1.8	3.5	-0.3	3.2	+0.61	3.74
8	4.7	early-K V	5000	2.1	6.8	-0.4	6.4	-0.67	3.69
24	5.4	M4 V	3370	5.3	10.7	-2.6	8.1	-1.35	3.53
36	4.4	M0 V	3850	3.7	8.1	-1.3	7.5	-1.11	3.59
37	4.7	M4 V	3370	5.3	10.0	-2.6	7.4	-1.07	3.53
40	2.2	K0 V	5250	2.0	4.2	-0.3	3.9	+0.33	3.72
42	3.5	late-K V	4000	3.2	6.7	-0.9	5.8	-0.43	3.60
43	1.9	K2-3 V	4800	2.3	4.2	-0.5	3.7	+0.41	3.68
44	5.0	M3 V	3470	4.7	9.7	-2.0	7.7	-1.19	3.54
46	5.2	M3 V	3470	4.7	9.9	-2.0	7.9	-1.27	3.54
51	3.9	M1 V	3720	3.9	7.8	-1.4	6.4	-0.67	3.57
56	-1.5	early-K III	–	–	–	–	–	–	–
78	3.4	M0 V	3850	3.7	7.1	-1.3	5.8	-0.43	3.59
86	3.7	early-M V	3720	3.9	7.6	-1.4	6.2	-0.59	3.57
105	4.6	M0-1 V	3800	3.9	8.5	-1.4	7.1	-0.95	3.58
111	3.3	late-K V	3950	3.2	6.5	-1.1	5.4	-0.27	3.59
112	1.3	early-K V	5080	2.1	3.4	-0.4	3.0	+0.69	3.71
113	2.8	late-K V	4000	3.2	6.0	-1.1	4.9	-0.07	3.60
115	2.9	early-M V	3720	3.9	6.8	-1.4	5.4	-0.27	3.57
118	2.0	early-K V	5000	2.1	4.1	-0.4	3.7	+0.41	3.70
120	0.9	early-K V	5000	2.1	3.0	-0.4	2.6	+0.85	3.70
121	2.7	mid-K V	4350	2.9	5.6	-0.7	4.9	-0.07	3.64
122	1.5	early-K V	5000	2.1	3.6	-0.4	3.2	+0.61	3.70
123	1.0	early-K V	5000	2.1	3.1	-0.4	2.7	+0.81	3.70
125	2.0	early−mid-K V	4730	2.4	4.4	-0.5	3.9	+0.33	3.67
128	1.7	late-K V	4000	3.2	4.9	-1.1	3.8	+0.37	3.60
130	0.0	late-B V	10500	-0.3	-0.3	-0.5	-0.8	+2.21	4.02

[a] ASR catalog number given in Paper I

[b] M_K is absolute K magnitude

[c] classification inferred from 2μm spectra and photometry

[d] effective temperature corresponding to spectral type from KH95

[e] source V-K colour from KH95

[f] absolute V magnitude

[g] visual bolometric correction from KH95

[h] visual bolometric magnitude

[i] Log_{10} luminosity in solar luminosities

[j] Log_{10} effective temperature

TABLE 8
MASSES AND AGES OF NGC 1333S SOURCES

ASR[a]	Mass ($M_\odot$)	Age (Years)
2	0.2	1×10^8
7	1.0	7×10^6
8	0.7	1×10^8
24	0.2	7×10^6
36	0.4	7×10^7
37	0.2	3×10^6
40	1.0	3×10^6
42	0.3	7×10^4
43	0.9	1×10^6
44	0.2	7×10^6
46	0.2	7×10^6
51	0.4	3×10^6
78	0.5	2×10^6
86	0.4	2×10^6
105	0.5	3×10^7
111	0.4	1×10^6
112	1.0	1×10^6
113	0.4	5×10^5
115	0.3	2×10^6
118	1.0	1×10^6
120	1.0	5×10^5
121	0.7	1×10^6
122	1.0	1×10^6
123	1.0	5×10^5
125	0.9	5×10^5
128	0.3	7×10^4
130	>2.0	$\geq1\times10^8$

[a] ASR catalog number given in Paper I

NOTE.—The range of masses and ages for ASR42 represent the range in inferred spectral types.

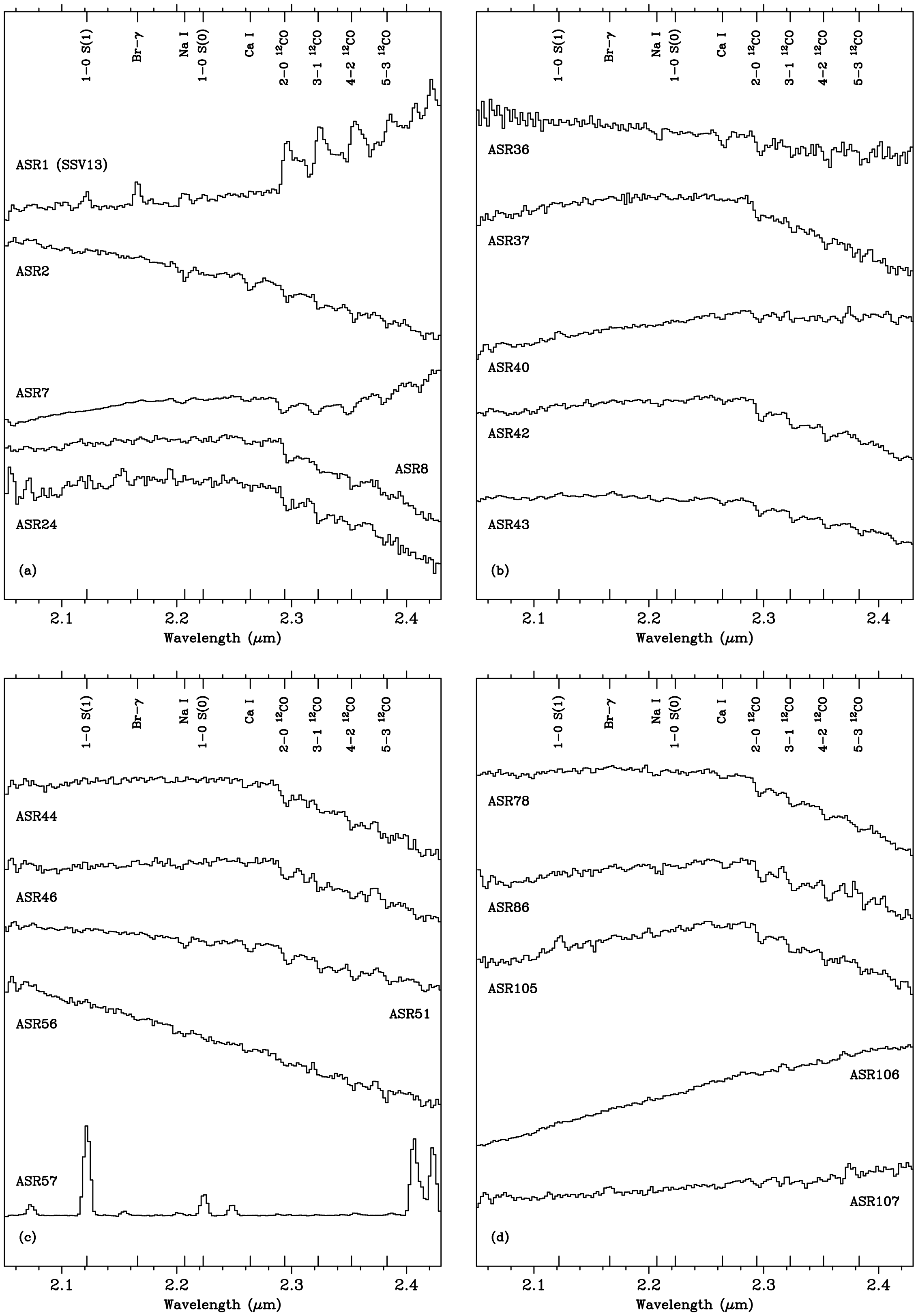

Fig. 1.— Spectra of sources in NGC 1333S. Each of the four plots (top-left 1a, top-right 1b, bottom-left 1c, bottom-right 1d) contains spectra of five sources. The wavelength range shown is 2.05–2.43μm. Each spectrum has been scaled to unit intensity at 2.25μm. The source fluxes are given in Table 2.

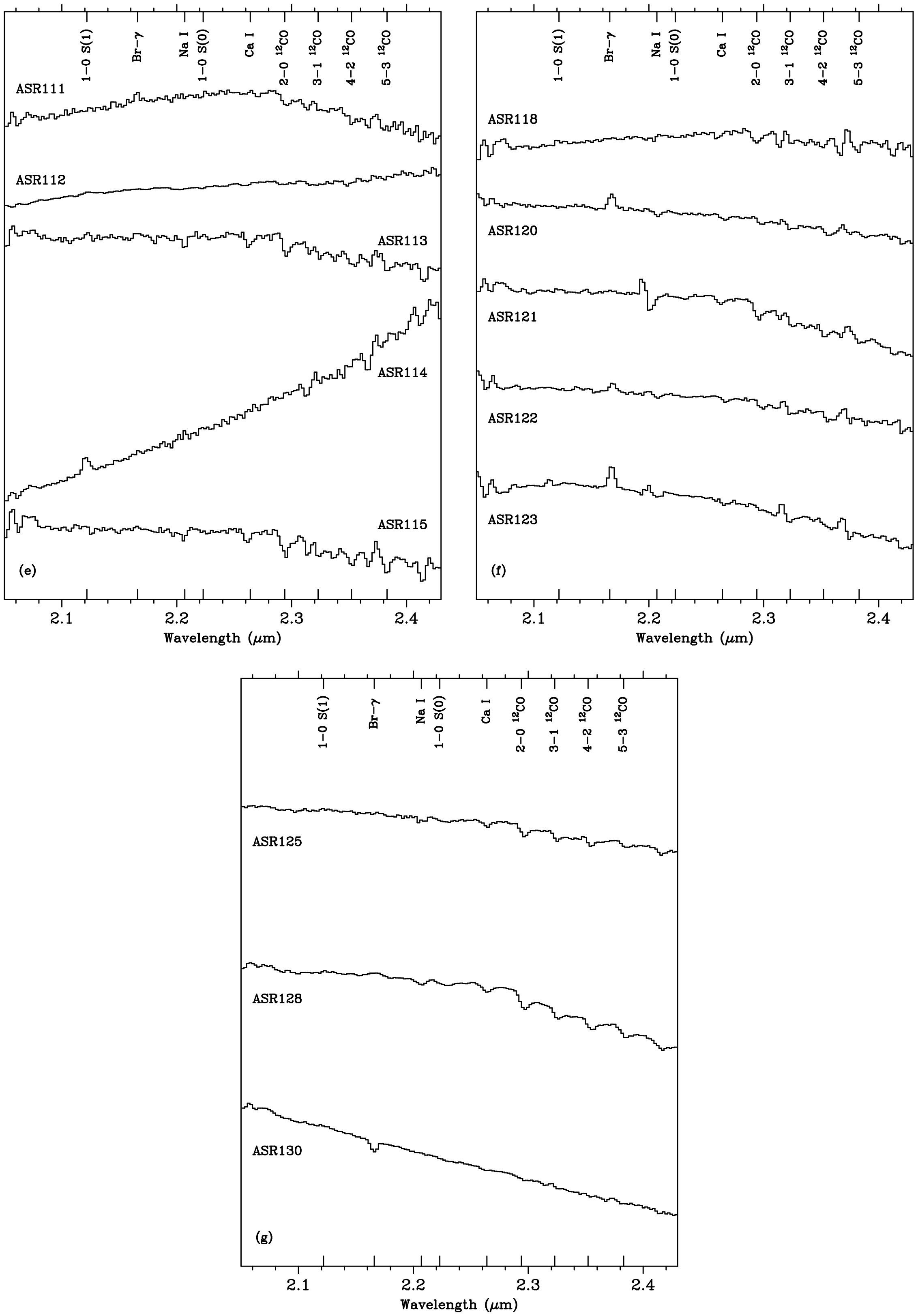

Fig. 2.— Spectra of sources in NGC 1333S. Each of the upper two plots (top-left 1a top-right 2b) contain spectra of five sources. The lower plot (bottom-centre 2c) contains spectra of three sources. The wavelength range shown is 2.05–2.43μm. Each spectrum has been scaled to unit intensity at 2.25μm. The source fluxes are given in Table 2.

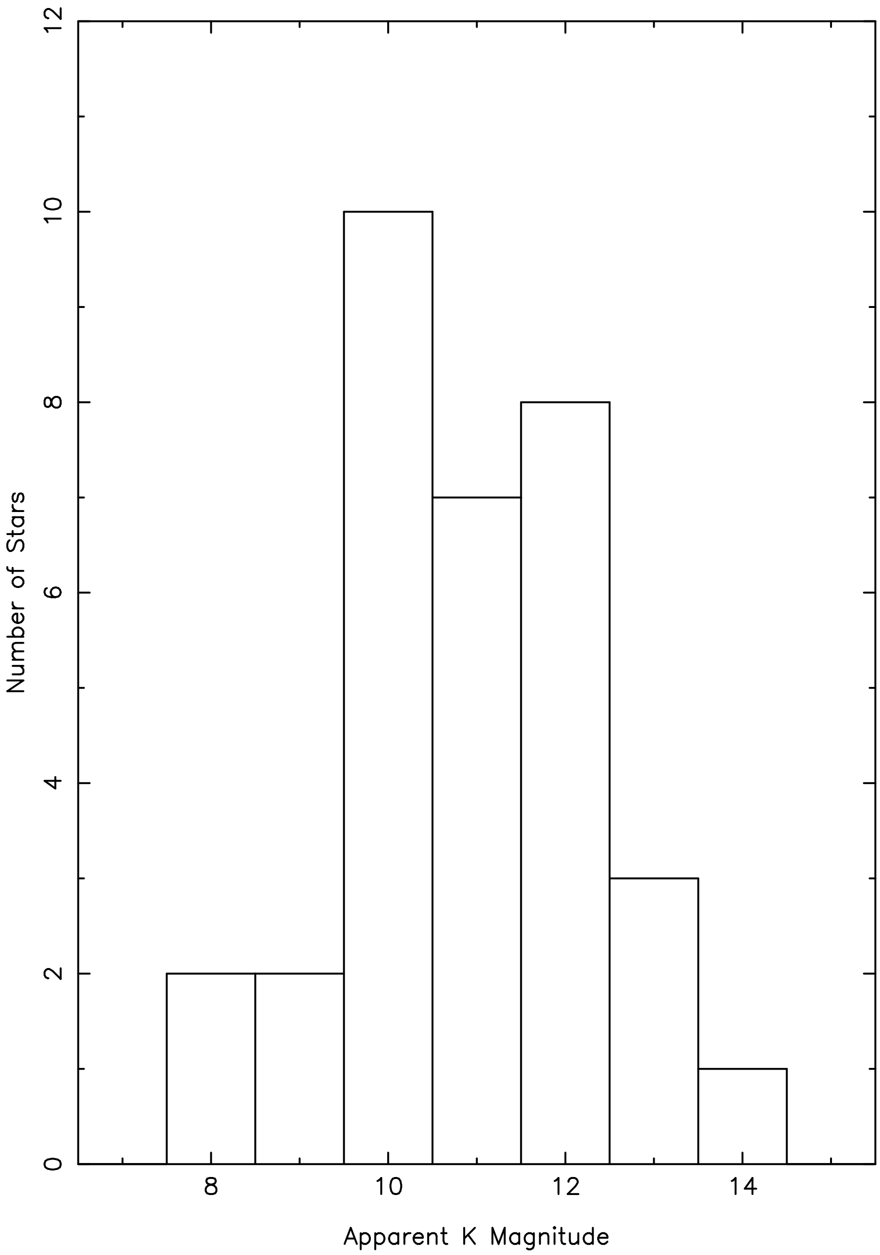

Fig. 3.— Histogram of the apparent K magnitude (m_K) of the sources observed in NGC 1333Susing 1 magnitude bins. The range of m_K is from 7.7 to 13.5 peaking at around 10–11.

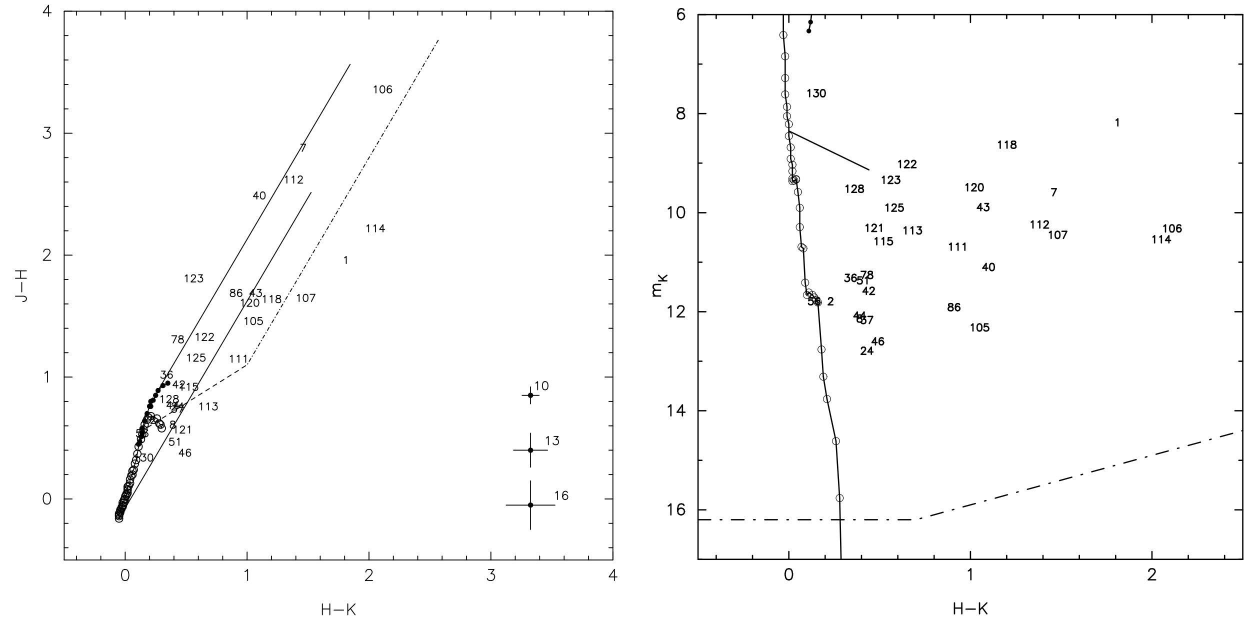

Fig. 4.— NIR J-H vs. H-K (JHK) colour-colour (c-c, left) and K vs. H-K (KHK) colour-magnitude (c-m, right) diagrams of the sources in NGC 1333S for which we have obtained 2μm spectra. The data shown is from Paper I. The number are the ASR source designations from Paper I and indicate the position of the source in the plot. In the c-c diagram, the curved lines with open and and filled circles are the loci of ZAMS stars (luminosity class V) and giant branch (luminosity class III) stars, respectively. The two solid lines are the Rieke & Lebofsky (1985) reddening vectors for A_V=20 magnitudes from the extremes of the ZAMS/giant branch. The dashed line represents the loci of colours of unreddened T Tauri Stars (TTS) taken from Greene & Meyer (1995, GM95) while the dot-dash line is the A_V=20 reddening line from the extreme TTS colour. In the c-m diagram, the ZAMS at 318pc is represented by the solid line with open circles and a reddening vector of A_V=7 is the solid line extending from the ZAMS at m_K $\sim$8.3

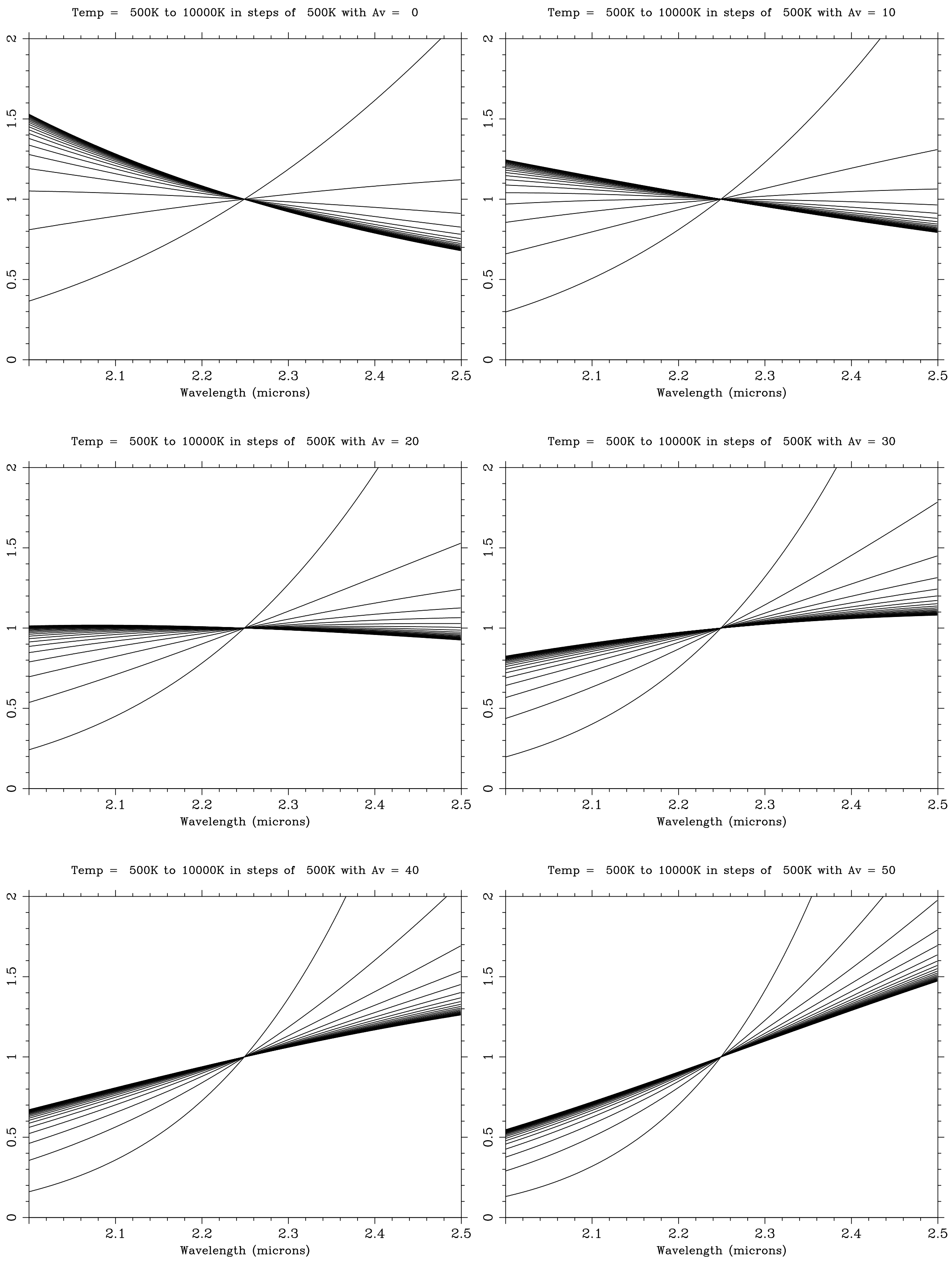

Fig. 5.— Plots of model reddened black-body spectra over the wavelength range 2–2.5μm for temperatures of 500K (steepest) to 10000K (shallowest) in steps of 500K. Top-left shows the unreddened A_V=0 spectra, top-right A_V=10, middle-left A_V=20, middle-right A_V=30, bottom-left A_V=40 and bottom-right A_V=50 magnitudes. This is the typical range of A_V values encountered in a embedded SFRs. For display purposes, the spectra have been normalized to unity at a wavelength of 2.25μm.

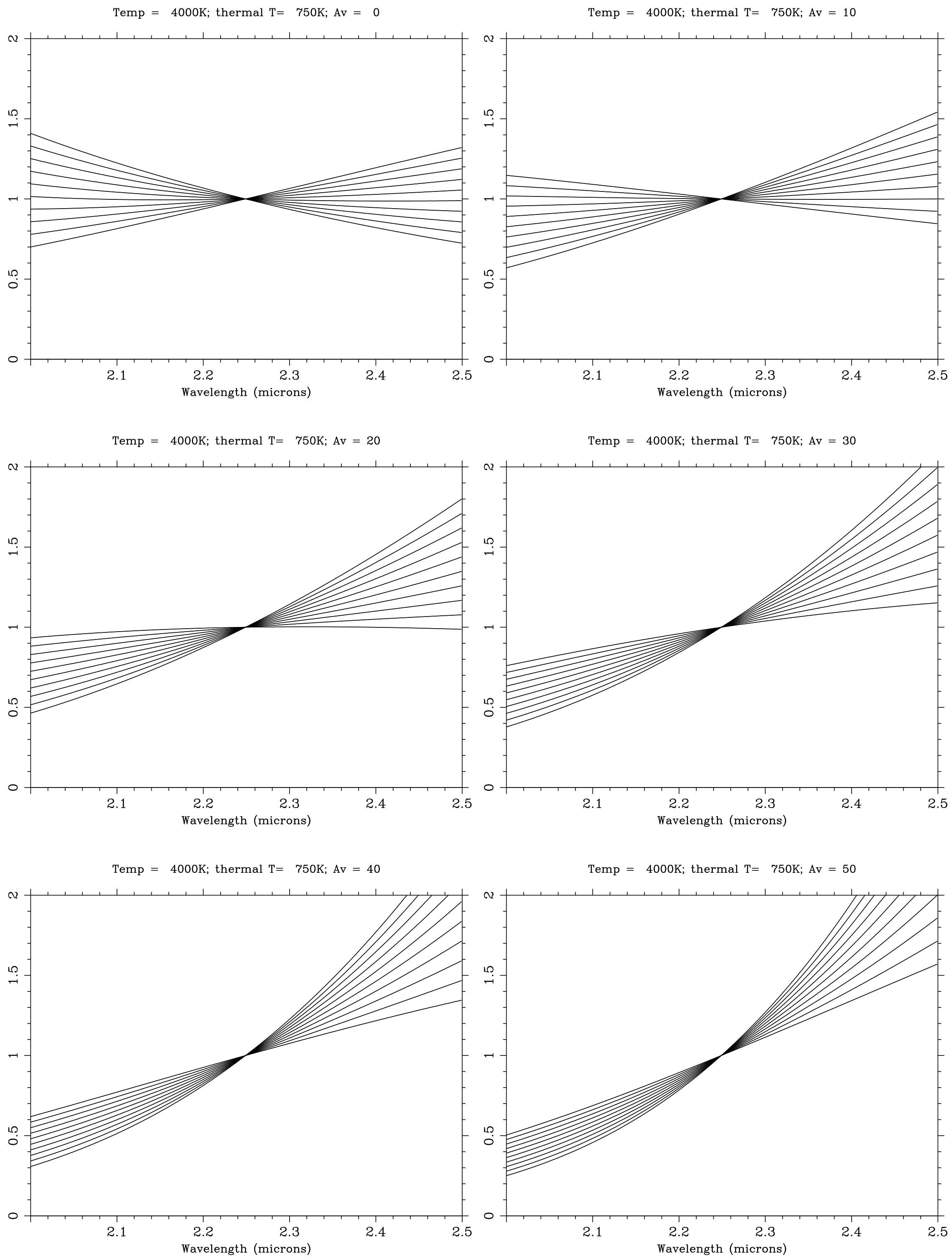

Fig. 6.— Plots of model reddened black-body spectra over the wavelength range 2–2.5μm for a photospheric temperature of 4000K with varying contributions from a 750K thermal emission component. In each plot the ratio of thermal to photospheric emission varies from 0 (shallowest) to 0.9 (steepest). Top-left shows the unreddened A_V=0 spectra, top-right A_V=10, middle-left A_V=20, middle-right A_V=30, bottom-left A_V=40 and bottom-right A_V=50 magnitudes. Again, for display purposes, the spectra have been normalized to unity at a wavelength of 2.25μm.

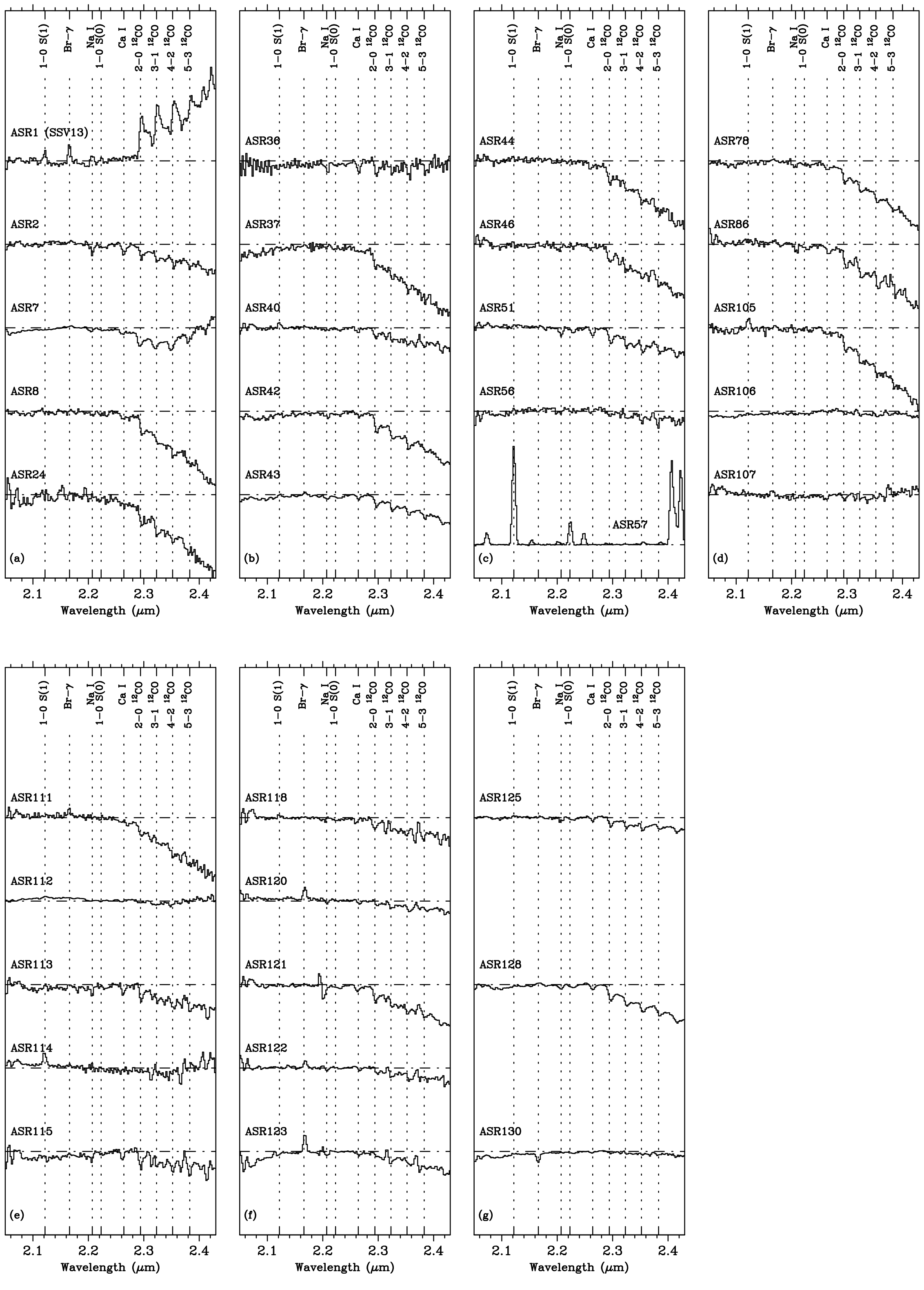

Fig. 7.— Plots of continuum subtracted target spectra. The parameters used in the definition of the continuum emission for each source are shown in Table 3. The vertical dotted lines indicate the main spectral features over the observed wavelength range. Note that some spectra are observed to turn down at 2μm. This is indicative broad of H_2O absorption in their spectrum and suggestive of the source being of later spectral type than M0 V.

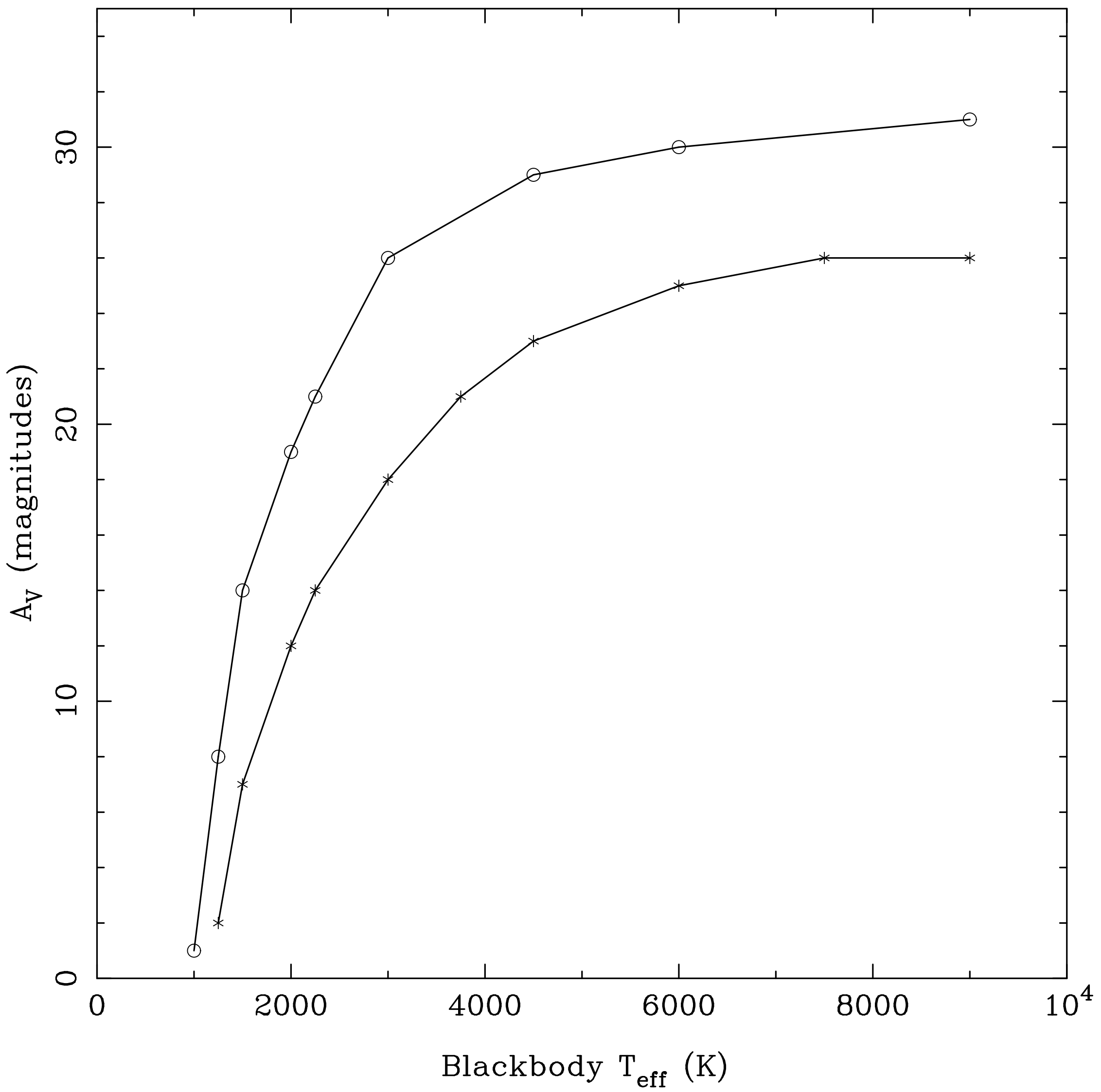

Fig. 8.— Plot of 'best fit' values of T_{der} and A_V for sources ASR 8 (stars) and ASR 40 (open circles). Planck functions with effective temperatures T_{eff} reddened by visual extinction A_V on each curve model the 2–2.5μm continuum of the sources equally well.

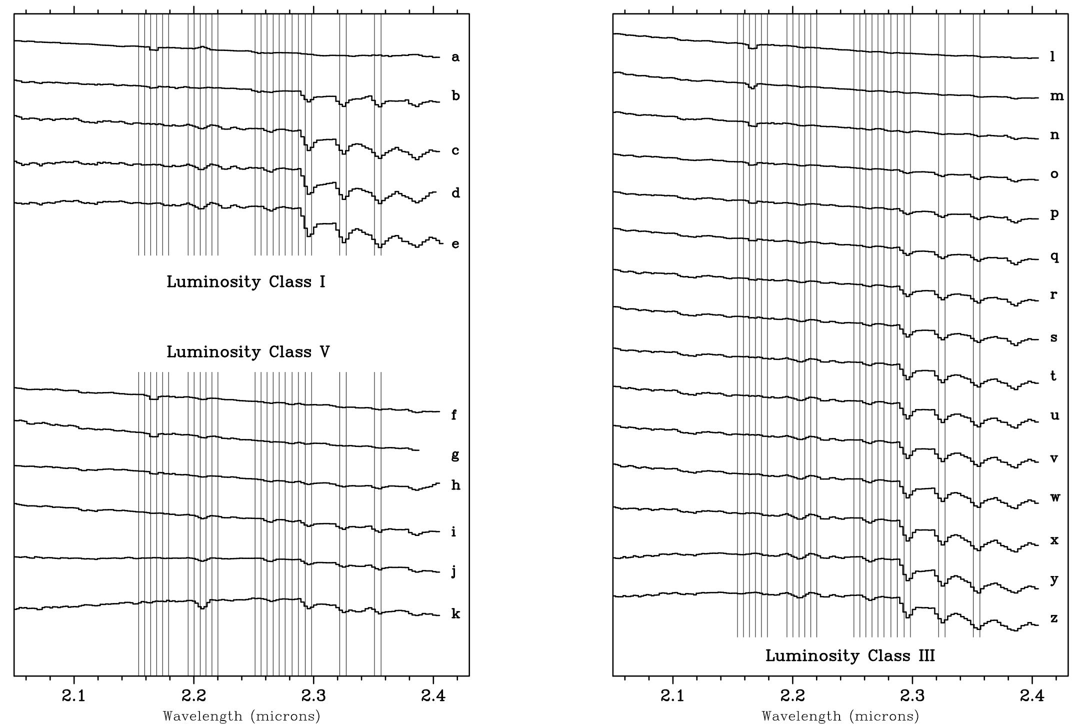

Fig. 9.— Plots of KH86 standard star spectra binned and smoothed to match the resolution in our target spectra. The thin vertical solid lines indicate the extremes of the integrated flux 'bins' used as diagnostics of stellar classification and luminosity class. The plots are labelled a to z where a is HR8752 (G5 0-Ia), b is RW Cep (K0 0-Ia), c is HR8726 (K5 Ib), d is μ Cep (M2 Ia), e is SU Per (M3-M4 Iab), f is 16 Cyg A (G3 V), g is 16 Cyg B (G4 V), h is σ Dra (K0 V), i is 61 Cyg A (K5 V), j is GL 411 (M2+ V), k is Wolf 359 (M5.8 V), l is ν Peg (F8 III), m is 31 Com (G0 III), n is 84 Her (G2 III), o is o UMa (G5 III), p is ϵ Vir (G8 III), q is ι Cep (K0- III), r is κ Oph (K2 III), s is 39 Cyg (K3 III), t is γ Dra (K5 III), u is γ Sge (M0- III), v is 75 Cyg (M1 III), w is *chi* Peg (M2 III), x is R Lyr (M5 III), y is BK Vir (M7 III) and z is SW Vir (M7 III).

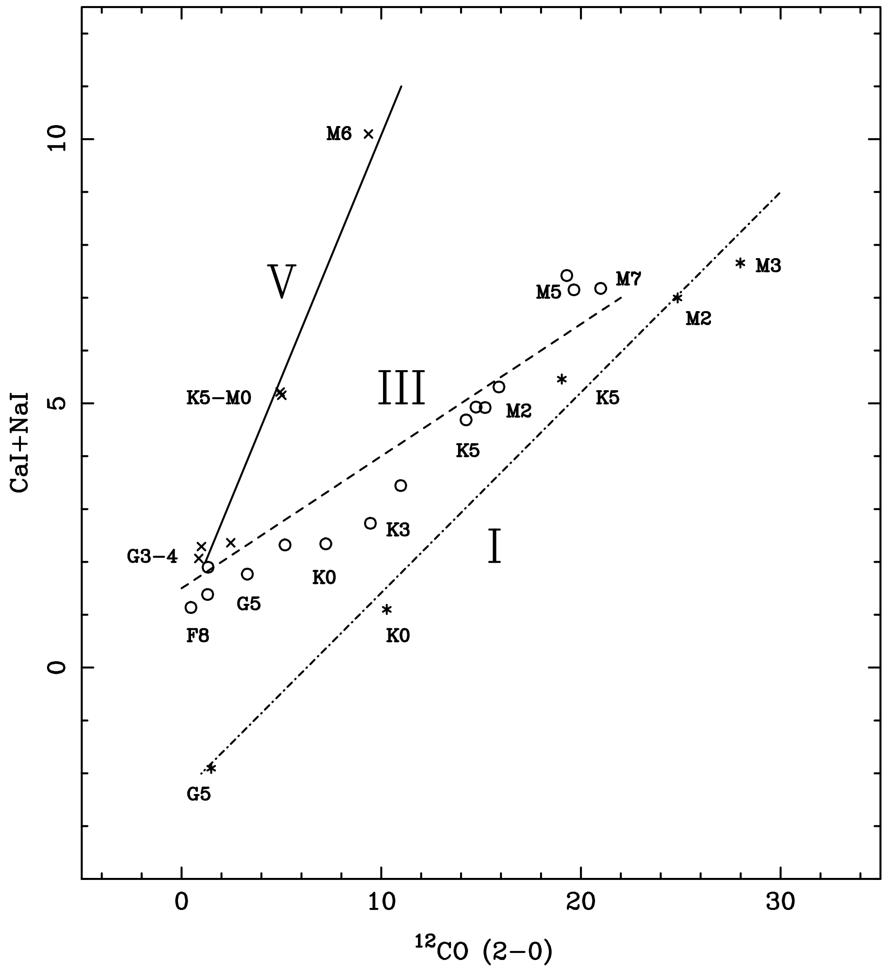

Fig. 10.— Plot of KH86 modified atomic index (Na I+Ca I) vs. molecular index (v=2-0 ^{12}CO) for the KH86 standard stars. Units are $\mathring{A}$ for both axes. The values shown were determined from the binned/smoothed spectra and show the same correlation as seen in the raw spectra plot of KH86 (see their Fig.7). The solid line, dot-dashed line and dashed line are the best-fit loci for luminosity class V main sequence dwarf stars (×), luminosity class III giants stars (o) and luminosity class I super-giant stars (*), respectively. Spectral types for some of the KH86 stars are shown next to the corresponding symbols.

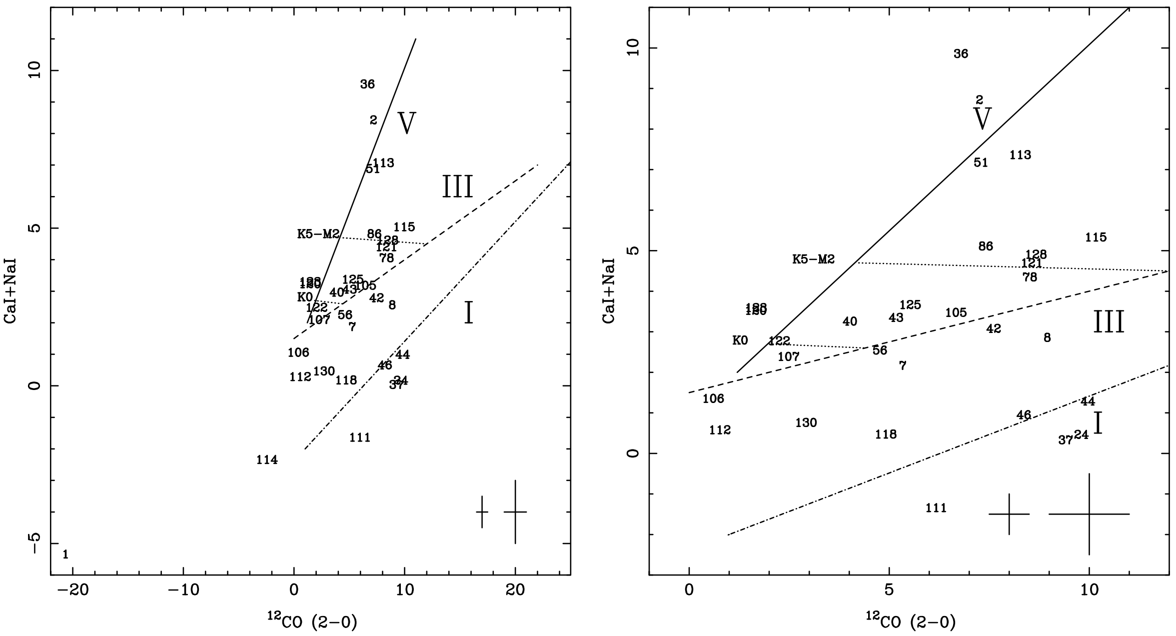

Fig. 11.— Plot of the KH86 modified atomic index (Na I+Ca I) vs. molecular index (v=2-0 ^{12}CO) index for the NGC 1333S sources. The loci shown are the same as in Fig. 10. Units are $\mathring{A}$ for both axes. Error are estimated to be $\sim \pm 0.5$ to ± 1.0 in both indices for large and small values, respectively. The source locations are represented by their ASR number. The two dotted lines represent stars of spectral classification K0 and K5-M2 from the dwarf (l.c. V) locus to the giant (l.c. III) locus (from the KH86 data, over the spectral range K5-M2 the atomic and molecular indices of dwarfs change by only a small amount). Representative 1σ error bars on the atomic and molecular indices are shown. The smaller error bars is for the brightest ASR sources while the larger error bar is for the faintest ASR sources.

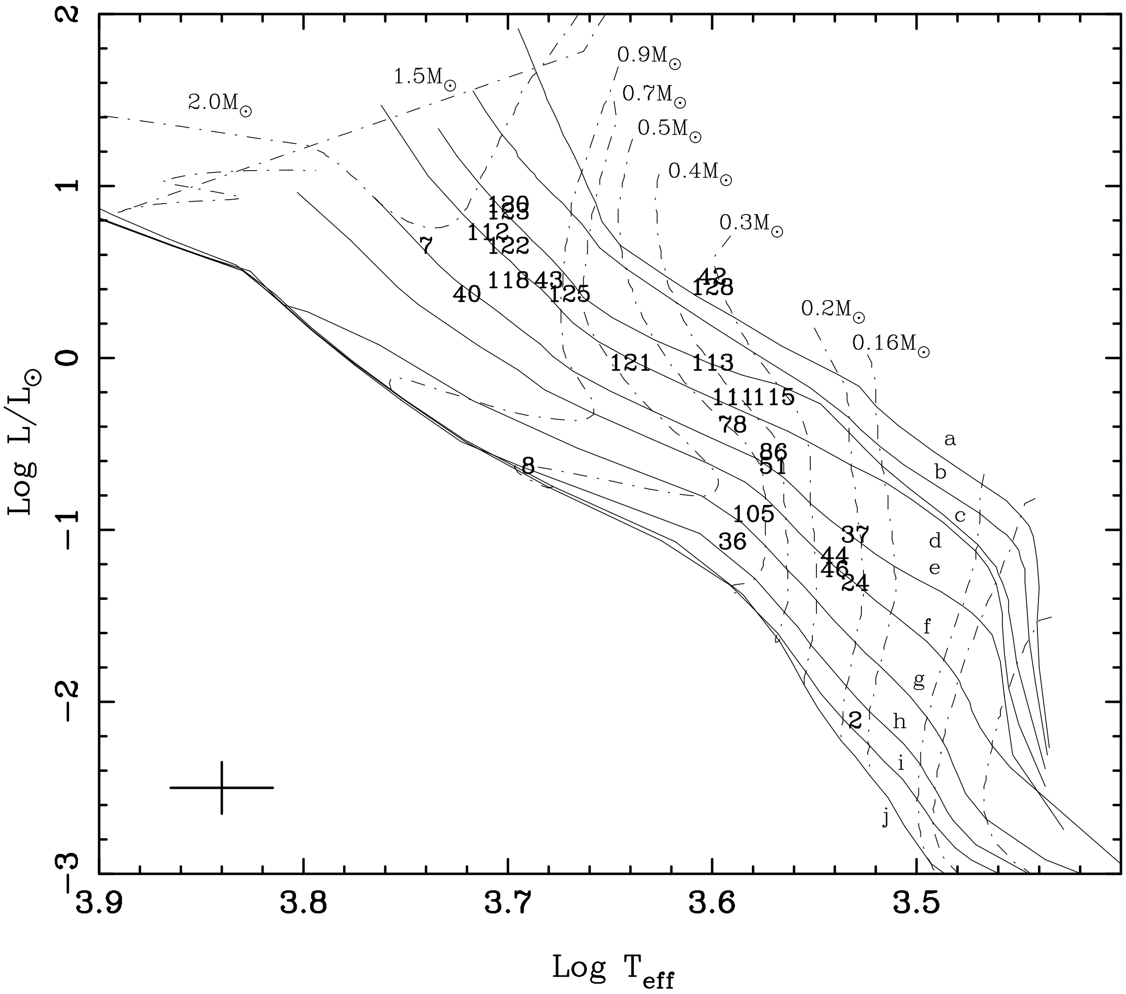

Fig. 12.— Hertzsprung-Russell diagram for the ASR sources overlaid on PMS evolutionary tracks and stellar isochrones from D'Antona & Mazzitelli (1997). Isochrones (solid lines) are plotted at ages 7×10^4 years (a), 2×10^5 years (b), 5×10^5 years (c), 1×10^6 years (d), 3×10^6 years (e), 7×10^6 years (f), 2×10^7 years (g), 5×10^7 years (h), 1×10^8 years (i) and 5×10^8 years (j). PMS tracks (dot-dash lines) for masses $0.16M_\odot$ to $2.0M_\odot$ are shown. The NGC 1333S source positions are indicated by their ASR numbers. The tracks/isochrones are for Y=0.26, Z=0.01 and $X_d=2\times10^{-5}$ with Alexander et al. (1989) opacities at $T_{eff}\leq$10000K and Rogers & Iglesias (1991) opacities for larger T_{eff}, and the Canuto & Mazzitelli (1990, 1992) CM convection model with a=0.5. ASR42 is included twice showing the range of possible values for its spectral classification of mid- to late-K V.